



Viscosity of crystal-free silicate melts from the active submarine volcanic chain of Mayotte

Pauline Verdurme, Charles Le Losq, Magdalena Oryaëlle Chevrel, Salomé Pannefieu, Etienne Médard, Carole Berthod, Jean-Christophe Komorowski, Patrick Bachèlery, Daniel R. Neuville, Lucia Gurioli

► To cite this version:

Pauline Verdurme, Charles Le Losq, Magdalena Oryaëlle Chevrel, Salomé Pannefieu, Etienne Médard, et al.. Viscosity of crystal-free silicate melts from the active submarine volcanic chain of Mayotte. Chemical Geology, In press, 620, pp.121326. 10.1016/j.chemgeo.2023.121326 . hal-03965373

HAL Id: hal-03965373

<https://uca.hal.science/hal-03965373>

Submitted on 31 Jan 2023

HAL is a multi-disciplinary open access archive for the deposit and dissemination of scientific research documents, whether they are published or not. The documents may come from teaching and research institutions in France or abroad, or from public or private research centers.

L'archive ouverte pluridisciplinaire **HAL**, est destinée au dépôt et à la diffusion de documents scientifiques de niveau recherche, publiés ou non, émanant des établissements d'enseignement et de recherche français ou étrangers, des laboratoires publics ou privés.



Distributed under a Creative Commons Attribution - NonCommercial - NoDerivatives 4.0 International License

Viscosity of silicate melts from the active submarine volcanic chain of Mayotte

Pauline Verdurme^{a,*}, Charles Le Losq^b, Oryaëlle Chevrel^a, Salomé Pannefieu^b, Etienne Médard^a, Carole Berthod^{a,b,c}, Jean-Christophe Komorowski^b, Patrick Bachèlery^a, Daniel R. Neuville^b and Lucia Gurioli^a

^a Université Clermont Auvergne, CNRS, IRD, OPGC, Laboratoire Magmas et Volcans, F-63000 Clermont-Ferrand, France

^b Université Paris Cité, Institut de physique du globe de Paris, CNRS, F-75005 Paris, France

^c Observatoire volcanologique et sismologique de la Guadeloupe, Institut de physique du globe de Paris, 97113, Gourbeyre, France

* Corresponding author:

E-mail address: pauline.verdurme@uca.fr

ORCID ID #: 0000-0003-1928-0009

Abstract

Following an unprecedented seismic activity that started in May 2018, a new volcanic edifice, now called Mont Fani Maoré, was constructed on the ocean floor 50 km east of the island of Mayotte (Indian Ocean). This volcano is the latest addition to a volcanic chain characterized by an alkaline basanite-to-phonolite magmatic differentiation trend. Here, we performed viscosity measurements on five silicate melts representative of the East-Mayotte Volcanic Chain compositional trend: two basanites from Mont Fani Maoré, one tephri-phonolite and two phonolites from different parts of the volcanic chain. A concentric cylinder viscometer was employed at super-liquidus conditions between 1500 K and 1855 K and a creep apparatus was used for measuring the viscosity of the undercooled melts close to the glass transition temperature. At super-liquidus temperatures, basanites have the lowest viscosity (0.11 - 0.99 log₁₀ Pa·s), phonolites the highest (0.91 - 3.89 log₁₀ Pa·s), while the viscosity of the tephri-

phonolite falls in between ($0.89 - 1.97 \log_{10} \text{ Pa}\cdot\text{s}$). Near the glass transition, viscosity measurements have only been performed for one phonolitic melt because obtaining pure glass samples for the basanitic and tephri-phonolitic compositions was unsuccessful due to the formation of nanolites as evidenced by Raman spectroscopy. The phonolite has a viscosity of 10.19 to $12.30 \log_{10} \text{ Pa}\cdot\text{s}$ at 1058 to 986 K . Comparison with existing empirical models revealed an underestimation of 1.2 to $2.0 \log$ units at super-liquidus and undercooled temperatures, respectively, for the phonolite. This emphasizes (i) the lack of data falling along the alkaline basanite-to-phonolite magmatic differentiation trend to calibrate empirical models, and (ii) the complexity of modeling the variations in viscosity as a function of temperature and chemical composition for alkaline composition. The presented new measurements indicate that, at eruptive temperatures between 1050°C and 1150°C (1323 - 1423 K), the oxidized, anhydrous, crystal-free and bubble-free basanite melt is very fluid with a viscosity around $1 \log_{10} \text{ Pa}\cdot\text{s}$. In contrast, the anhydrous phonolitic crystal- and bubble-free melt at eruptive temperatures ranging from 800 to 1000°C (1073 - 1273 K) would have a viscosity around $6 - 10 \log_{10} \text{ Pa}\cdot\text{s}$. Considering that both basanitic and phonolitic melts from the Mayotte submarine volcanic chain contain less than 6% crystals and a significant amount of water, such viscosity values are probably upper limits. These new viscosity measurements are essential to define eruptive models and to better understand the storage and transport dynamics of Comoros Archipelago magmas, and of alkaline magmas in general, from the source to the surface.

keywords

viscosity, alkali magmas, submarine volcano, volcanic eruption, Raman spectroscopy

1. Introduction

Following an unprecedented intense seismic crisis that started in May 2018 ([Lemoine et al. 2020](#); [Feuillet et al. 2021](#)), surveys revealed a new submarine volcanic edifice, recently named Mont Fani Maoré, 936 m tall with a base at around 3,500 m depth, 50 km east of Mayotte (Indian Ocean). This large eruption has extruded around 6.55 km³ of basanite magma, with first estimates of magma transfer rates from source to surface of a minimum of 30 days ([Cesca et al. 2020](#); [Berthod et al. 2021a](#)). The source of this magma is evaluated to be located at 30 - 50 km depth into the underlying mantle, with the potential involvement of an intermediate magma chamber located at ~17 km depth ([Berthod et al. 2021b](#)). This new volcano is an addition to the East-Mayotte Volcanic Chain, characterized by the emission of magmas falling along an alkaline basanite-to-phonolite magmatic differentiation trend. This volcanic chain is quite complex and characterized by large effusive lava flow fields, and by the presence of more explosive volcanoes ([Figure 1](#)) ([Puzenat et al. 2022](#); [Gurioli et al. 2023](#); [Komorowski et al. 2023](#)). To better understand and constrain the storage processes and transfer rates of the magmas that feed the East-Mayotte Volcanic Chain and the dynamics of their emplacement at surface, it is necessary to constrain the viscosity of the basanite-to-phonolite melts, which determines the mobility of magmas toward the surface as well as their fragmentation behavior in the conduit and flow at the surface ([Dingwell et al. 1996](#); [Papale 1999](#); [Pistolesi et al. 2011](#)). To constrain the viscosity of magmas and lavas, one can potentially rely on the various experimental and modeling efforts that led to important improvements in our knowledge of how it is controlled by temperature ([Vogel 1921](#); [Tamman and Hesse 1926](#); [Fulcher 1925](#); [Adam and Gibbs 1965](#); [Nascimento and Aparicio 2007](#)), chemical composition ([Bottinga and Weill 1972](#); [Shaw 1972](#); [Giordano et al. 2008](#)), volatile elements (e.g., [Whittington et al. 2000](#), [2001](#)), bubbles ([Lejeune et al. 1999](#); [Llewelin and Manga et al. 2005](#)) and crystal contents ([Lejeune and Richet 1995](#); [Kolzenburg et al. 2022](#)). Yet, there is not a general and very accurate

magma viscosity model to date, due to the complexity in estimating the influence of the different parameters listed above. Focusing only on the silicate melt phase of magmas and lavas, many effects exist at the atomic level, such as aluminum coordination changes or metal cation mixing, that result in strong and non-linear variations in melt viscosity depending on composition. In particular, in alkali-rich melts, the way Na and K mix may strongly affect viscosity (Poole, 1948; Richet, 1984; Le Losq and Neuville, 2013, 2017). In Al-poor melts, the ideal mixing between Na and K results in an important decrease in viscosity (Richet 1984), whereas in Al-rich melts, Na and K occupy different environments and do not mix ideally (Le Losq and Neuville 2013, 2017; Le Losq et al. 2021). At a given temperature, this leads to increasing the melt viscosity by several orders of magnitude upon increasing the melt K/(K+Na) ratio. Existing parametric viscosity models (e.g., Hui and Zhang 2007; Giordano et al. 2008) failed to properly reproduce such an effect (Le Losq and Neuville 2013; Robert et al. 2019). Therefore, their accuracy for the prediction of the viscosity of melts along alkaline magmatic series is to be improved. Only models integrating thermodynamic and physico-chemical knowledge allow to properly model the way Na and K non-ideal mixing alter the viscosity of Al-rich alkali melts. However, this has been applied only on quaternary alkali aluminosilicate melts far from natural compositions (Robert et al. 2019; Starodub et al. 2019; Le Losq et al. 2021, Neuville and Le Losq 2022). Therefore, to properly constrain the viscosity of alkali melts, one needs to use *ad hoc* models for increased precision, as it has been performed for the phonolite of Erebus volcano (Antarctica) for instance (Le Losq et al. 2015a).

In this contribution, we present new viscosity measurements performed on samples representative of the lava compositions that can be found along the East-Mayotte submarine volcanic chain. Those samples fall along the moderately silica-undersaturated trend (“Karthala-trend”) of the Comoros Archipelago (Pelleter et al. 2014; Bachèlery et al. 2016; Bachèlery and Hémond 2016). The studied compositions include two basanite lavas from the recent eruption

(Mont Fani Maoré volcano), and two phonolite and a tephri-phonolite samples from other emission sites in the submarine volcanic chain (Berthod et al. 2021a; Feuillet et al. 2021; Puzenat et al. 2022; Figure 1). Viscosity is measured with a concentric cylinder viscometer at super-liquidus temperatures, in the 10^0 - 10^6 Pa·s range, and with a creep apparatus close to the glass transition temperature between 10^8 and 10^{13} Pa·s. We also examine the effect of the water content on the viscosity of the different magma compositions present at Mayotte. The results (i) provide the foundation necessary to investigate the eruptive behavior of the Mayotte volcanic system, (ii) strengthen the current knowledge on alkaline series and (iii) could contribute to refine the pre-existing empirical viscosity models based on chemical composition.

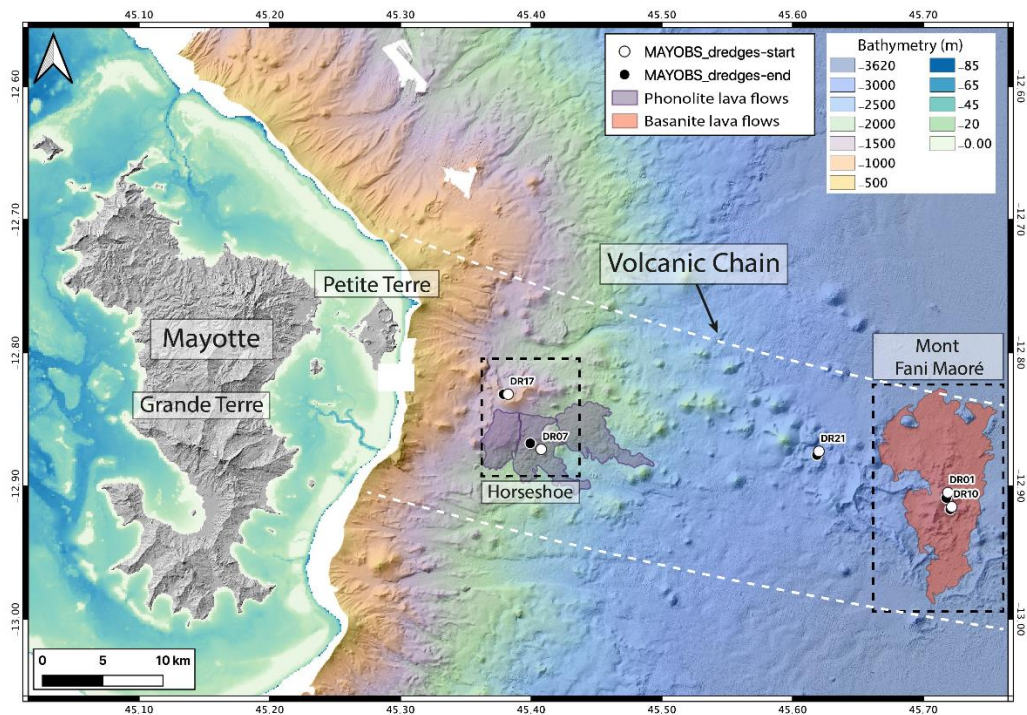


Figure 1. Geological map of the submarine volcanic chain of Mayotte showing the location of the dredged samples (DR labels). Mont Fani Maoré lava flows are modified from Feuillet et al. (2021). Modified from Berthod et al. (2021a). Background is the bathymetry from the Homonim project (SHOM 2015), DEM Litto3D IGN-SHOM (SHOM 2016) and MAYOBS1 (doi:10.17600/18001217).

2. Materials and Methods

2.1. Starting material

In this study, the investigated samples were collected by dredging operations that collected between 100 - 1000 kg of rocks, from water depths ranging from 1,370 to 3,455 m (**Figure 1**). These dredges were operated by the R/V *Marion Dufresne II* and R/V *Pourquoi Pas?* during the following oceanographic cruises (**Rinnert et al., 2019**): MAYOBS 1 (**Feuillet, 2019**), MAYOBS 2 (**Jorry 2019**), MAYOBS 4 (**Fouquet and Feuillet, 2019**), MAYOBS 15 (**Rinnert et al., 2020**), and GEOFLAMME (**Rinnert et al., 2021**) (**Table 1**).

Table 1. *Location of the dredges performed during the oceanographic cruises. Latitudes and Longitudes are given in decimal degrees (DD).*

| Dredges | Oceanographic cruises | DOI of the oceanographic cruises 10.18142/291 | Start dredging | | | End dredging | | |
|---------|-----------------------|--|----------------|-----------|--------|--------------|-----------|--------|
| | | | Latitude | Longitude | Depth | Latitude | Longitude | Depth |
| DR01 | MAYOBS 1 | 10.17600/18001217 | -12.905 | 45.719 | 3050 m | -12.909 | 45.718 | 2820 m |
| DR07 | MAYOBS 2 | 10.17600/18001222 | -12.872 | 45.407 | 1590 m | -12.868 | 45.399 | 1585 m |
| DR10 | MAYOBS 4 | 10.17600/18001238 | -12.916 | 45.722 | 3120 m | -12.918 | 45.721 | 2950 m |
| DR17 | MAYOBS 15 | 10.17600/18001745 | -12.831 | 45.382 | 1370 m | -12.831 | 45.379 | 1340 m |
| DR21 | GEOFLAMME | 10.17600/18001297 | -12.874 | 45.620 | 2719 m | -12.876 | 45.618 | 2629 m |

We selected five samples that represent the diverse composition of the volcanic deposits along the Mayotte submarine volcanic chain (**Fig. 1** and **Table 2**). Two samples (MAY01-DR010101 and MAY04-DR100504, hereafter named DR01 and DR10, respectively) are from Mont Fani Maoré, the new volcano that has been in activity from 2018 to 2021 (**Fig. 1**, **Lemoine et al.**

2020; Berthod et al. 2021b; Feuillet et al. 2021). These two samples are fragments of basanite lava flows collected on the central edifice and were emitted during the first year of the eruption (before May 2019, Berthod et al., 2021b). Two other samples (MAY02-DR070201 and MAY15-DR170404, hereafter named DR07 and DR17, respectively) were recovered at 10 - 15 km east of Petite Terre Island of Mayotte on the “Horseshoe” volcanic structure (Fig. 1, Berthod et al. 2021a; Feuillet et al. 2021; Puzenat et al. 2022; Gurioli et al. 2023). DR07 is a fragment of a Holocene phonolitic lava flow located on the southeastern part of the Horseshoe site. DR17 is a phonolitic pyroclast bomb collected at the bottom of the internal western side slope of the Horseshoe structure. Finally, the fifth sample (GFL-DR2110, hereafter named DR21) was collected on a seamount located in the middle of the submarine volcanic chain, 10 km west of Mont Fani Maoré (Rinnert et al., 2021). This sample is a fragment of lava and has a tephri-phonolitic composition.

About 200 g of each sample were used to produce the starting glasses necessary for the experiments. The rock samples were first crushed and powdered. A portion of the powder was used for bulk rock chemical analyses and the rest for viscosity measurements. Chemical analyses have also been performed on the glass chips produced after high- and low-temperatures viscometry.

2.2. Major element analyses

Bulk rock major element composition of the starting materials was analyzed at Laboratoire Magmas et Volcans (LMV, Clermont-Ferrand, France). Samples were crushed into millimeter-size chips using home-made thermally hardened steel jaws, and powdered in a motorized agate mortar. Major elements were analyzed by Inductively Coupled Plasma Atomic Emission Spectrometry (ICP-AES). Powdered samples were melted with LiBO₂ in a magnetic induction oven at 1100 °C for 5 min using graphite crucibles. The glass beads were then dissolved in a

solution of deionized water and nitric acid (1 M) and diluted by a factor of 2000 to produce the solution analyzed by an Agilent 5800 VDV ICP AES in radial mode. Analytical uncertainties ($\pm 2\sigma$) vary between 1 and 3 % except for K₂O, MnO (4 %) and P₂O₅ (7 %) for the DR-N standard (diorite). For the analysis, the plasma flow was 12 L/min, the nebulizer flow was 0.7 L/min and the radio frequency power was 1.2 kW.

Glass chips resulting from spindle quench after the super-liquidus viscometry were mounted as polished sections for chemical analysis carried out with the CAMECA SX Five Tactis electron microprobe at LMV. We used an accelerating potential of 15 kV at current of 8 nA, with a defocused beam of 20 μ m diameter to avoid Na migration under the electron beam. Natural and synthetic mineral standards, including orthoclase (K, Al), albite (Na), wollastonite (Si, Ca), fayalite (Fe), forsterite (Mg), TiMnO₃ (Ti, Mn), NiO (Ni), Cr₂O₃ (Cr), and fluorapatite (P) were used for routine calibration.

We also calculated the NBO/T parameter (number of non-bridging oxygens per tetrahedral), representing the degree of polymerization of the melt following [Mysen et al. \(1982\)](#):

$$\frac{NBO}{T} = \frac{(2O)-(4T)}{T}, \quad (1)$$

with O the atomic proportion of oxygen atoms and T that of cations entering as network formers in tetrahedral coordination, namely SiO₂, TiO₂, Al₂O₃, and Fe₂O₃ (see for a review of such concepts [Le Losq et al. 2019; Neuville and Le Losq 2022](#)). Here, the total iron is expressed as Fe³⁺ as the viscosity experiments were performed in an oxidizing environment. This assumption is a valid simplification: estimations with the [Moretti \(2005\)](#) model yields 90 % or more of Fe residing in the melt as Fe₂O₃ at the conditions of our experiments. The NBO/T of the natural melt may thus be higher, considering the occurrence of reduced iron and its influence on the melt structure (e.g., [Le Losq et al. 2021](#)).

2.3. High temperature viscometry

High temperature viscosity measurements are performed at super-liquidus conditions, in air, using a concentric cylinder viscometer (Dingwell 1986; Spera et al. 1988) at the Institut de physique du globe de Paris (IPGP, Paris, France). Powdered glass samples are first melted at 1800 K in a Pt₉₅Au₅ cylindrical crucible (50 mm height, 27 mm inner diameter, 1 mm wall thickness) in a muffle furnace. Once the crucible is full, it is inserted in the hot zone of the viscometer vertical tube furnace, heated by Super Kanthal 33 elements in air. The length of the hot zone was determined by temperature measurement inside the crucible: the vertical and radial temperature gradients inside the crucible are respectively less than 2 K for 5 cm (vertical gradient) and 1 K for 2.7 cm (radial gradient) at 1500 K and a little less at 1800 K. The inner rotating spindle size is 14 mm in diameter, 21 mm in height and has 23° conical extremities to reduce termination effects and a 5 mm diameter stem. Viscosity is measured using a Rheomat 115 rheometer head, which allows rotating the cylinder at angular velocities ranging between 0.05 and 780 rpm (Neuville 2006). The torque exerted on the cylinder by the sample is recorded digitally. The correspondence between the exerted torque and the viscosity is calibrated against the reference sample NBS SRM 710a, for which the viscosity–temperature relationship is accurately known (Neuville 2006). The accuracy is of the order of 0.02 log Pa·s (e.g., Neuville 2006).

2.4. Low temperature viscometry

Low temperature viscosity measurements are performed near the glass transition temperature (T_g) using a creep apparatus at IPGP (Neuville and Richet 1991; Neuville 2006). Glass samples used for measurements are (i) a parallelepiped of 7.9 mm length, and (ii) a small cylinder of 2.2 mm diameter x 8.1 mm length. A silver cylinder is placed around the sample, creating a small chamber in which temperature is homogeneous. Lateral and vertical temperature

gradients are controlled using two Pt-PtRh₁₀ thermocouples (ITS90 type S thermocouples); before and during each measurement, lateral and vertical temperature gradients were always lower than 0.2 K. To measure sample viscosity at a given temperature, we performed 20 to 30 measurements at different stresses (between 6.4 and 8.2 log Nm⁻²) to check for the occurrence of a non-Newtonian behavior, which could be a sign of crystallization of the sample. Each reported viscosity value at a given temperature is the statistical mean of these measurements. Measurements carried out on the NBS 717 glass show that errors on viscosity measurements are lower than 0.03 log Pa·s with this apparatus (e.g., [Neuville 2006](#)).

2.5. Raman spectroscopy

The Raman spectra of the glasses (pre- and post-experiments) were recorded with the Labram HR Evolution spectrometer available at IPGP, equipped with a Peltier-cooled CCD and a 1800 lines mm⁻¹ grating. The samples were excited with a Coherent MX 488 nm solid-state laser focused through a ×50 Olympus objective on the sample surface. The confocal aperture of the spectrometer was set to 50. With this setup, spectral resolution is ~3 cm⁻¹ and spatial resolution is ≤1 cm⁻¹. All spectra were recorded with the laser focused at 3-5 μm below the sample's surface to avoid any surface effects ([Behrens et al. 2006](#), [Schiavi et al. 2018](#)). The laser power on the sample has been adjusted to lower than 10 mW to avoid any potential damage on the sample (iron oxidation effects or melting). Potential damage was checked by recording several spectra on the same spot and varying laser power, without the identification of any effect. Raman data treatment was performed using the Python programming software, with the *rampy* open-source software library ([Le Losq 2018](#)).

3. Results

3.1. Major element composition

The bulk rock chemical composition of the pre-experiment samples and the post-experiments glass compositions, determined by ICP-AES and by electron microprobe analyses respectively, are reported in **Table 2** and presented in **Figure 2**.

DR01 and DR10 basanites have a very similar composition between 47.1 and 47.7 wt% SiO₂ and 7.2 to 7.8 alkali (Na₂O + K₂O) wt% (**Fig. 2**). These samples have low MgO contents, between ~4.8 and ~5.4 wt%, and high FeO_{tot.} contents, between ~12.5 and ~12.7 wt% (**Table 2**), making them the most iron-rich among all the studied samples from the East-Mayotte submarine volcanic chain. DR07 and DR17 phonolite samples have similar silica content of 57.7 - 58.9 wt% SiO₂ but DR07 has an alkali content of 13.0 wt% while DR17 is more enriched in alkali with 14.2 wt% (**Fig. 2** and **Table 2**). Compared to basanite samples, phonolite samples have lower FeO_{tot.} contents, ranging from 6.1 to 7.2 wt%. Finally, sample DR21 has a tepri-phonolitic composition, falling in between the basanite and phonolite fields of the TAS diagram (**Fig. 2**) with SiO₂ and alkali contents of 53.2 wt% and 10.8 wt%, respectively (**Table 2**) and an intermediate FeO_{tot.} content of 10 wt%.

For most samples, the major element contents show no significant differences before and after viscosity experiments (**Table 2**). We however note that the composition of DR17 after the high-temperature experiment has a slightly higher SiO₂ content of 1.5 wt%. This is accompanied by iron loss of 0.5 wt% (**Table 2**).

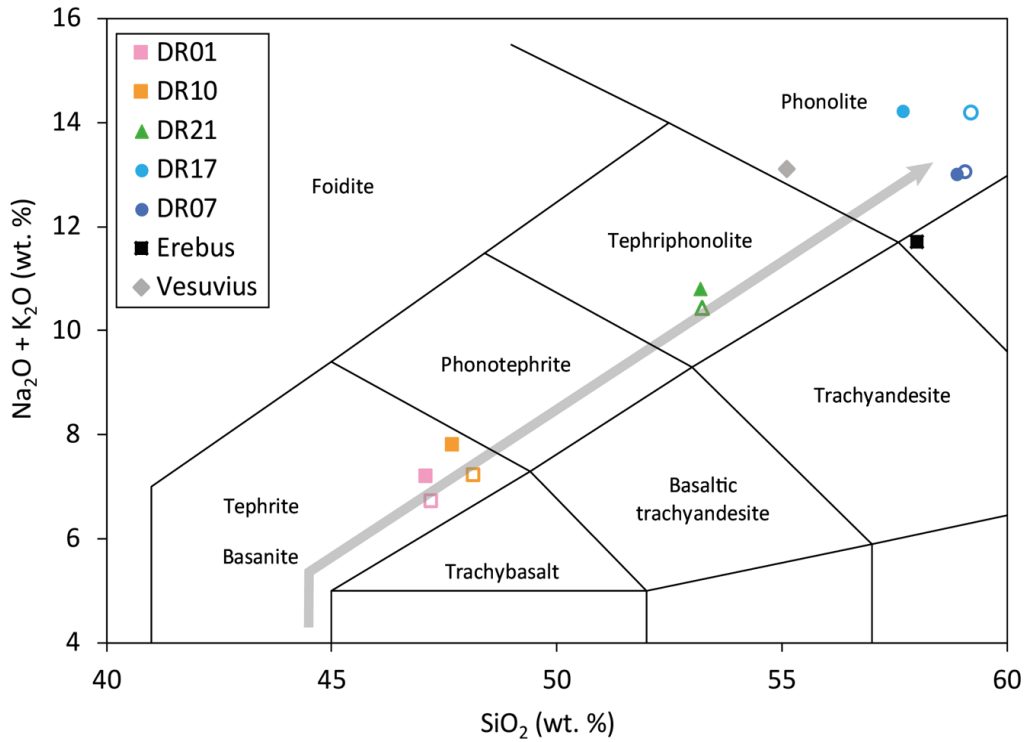


Figure 2. TAS diagram showing normalized compositions of the studied samples before (filled symbols, ICP-AES) and after (empty symbols, Electron Microprobe) viscosity measurements. Compositions of phonolite lavas from Erebus and Vesuvius (GP79, Grey Pumice of the 79 eruption) are also shown for comparison (data from [Le Losq et al. 2015a](#)). The grey arrow shows the moderately silica-undersaturated trend (“Karthala-trend”) identified by [Pelleter et al. \(2014\)](#) and [Bachèlery and Hémond \(2016\)](#). Error bars are smaller than symbol size.

Table 2. Normalized major element composition in wt% pre- (first line) and post- (second line) experiments of the studied samples. The post-experiment composition are an average of at least ten measurements made on glass. The composition of Erebus and Vesuvius GP79 from [Le Losq et al. \(2015a\)](#) are also reported for comparison.

| Sample | SiO ₂ | TiO ₂ | Al ₂ O ₃ | FeO(t) | MnO | MgO | CaO | Na ₂ O | K ₂ O | P ₂ O ₅ | NBO/T |
|-------------------------------------|------------------|------------------|--------------------------------|--------|-----|-----|-----|-------------------|------------------|-------------------------------|-------|
| <i>Before and after experiments</i> | | | | | | | | | | | |
| DR01 | 47.1 | 3.3 | 15.3 | 12.7 | 0.2 | 5.4 | 7.3 | 4.7 | 2.5 | 1.6 | 0.3 |
| | 47.2 | 3.4 | 14.8 | 13.2 | 0.3 | 5.4 | 7.3 | 4.4 | 2.4 | 1.6 | - |
| DR10 | 47.7 | 3.1 | 15.2 | 12.5 | 0.2 | 4.8 | 6.8 | 5.2 | 2.6 | 1.9 | 0.3 |
| | 48.1 | 3.2 | 15.3 | 12.6 | 0.3 | 4.9 | 6.8 | 4.6 | 2.6 | 1.7 | - |
| DR21 | 53.2 | 1.6 | 16.5 | 9.8 | 0.3 | 1.9 | 4.2 | 6.8 | 4.0 | 1.0 | 0.2 |
| | 53.2 | 1.7 | 16.9 | 10.0 | 0.3 | 2.0 | 4.5 | 6.5 | 4.0 | 1.0 | - |
| DR07 | 58.9 | 0.4 | 18.2 | 7.2 | 0.3 | 0.4 | 1.6 | 7.6 | 5.4 | 0.3 | 0.1 |
| | 59.1 | 0.4 | 18.6 | 6.4 | 0.3 | 0.3 | 1.6 | 7.6 | 5.7 | 0.3 | - |
| DR17 | 57.7 | 0.1 | 18.7 | 6.1 | 0.3 | 0.1 | 1.3 | 8.6 | 5.6 | 0.1 | 0.1 |
| | 59.2 | 0.1 | 19.1 | 5.6 | 0.2 | 0.1 | 1.3 | 8.4 | 5.8 | 0.1 | - |
| Erebus melt | 58.0 | 1.0 | 20.0 | 5.4 | 0.2 | 0.9 | 2.6 | 7.1 | 4.6 | 0.0 | 0.1 |
| Vesuvius GP79 | 55.1 | 0.5 | 19.5 | 4.1 | 0.1 | 1.8 | 5.3 | 4.4 | 8.7 | 0.0 | 0.3 |

The calculated NBO/T values of the oxidized melts range from 0.1 to 0.3 (**Table 2**). DR01 and DR10 basanite samples have the highest NBO/T (0.32 and 0.33). On the other hand, DR07 and DR17 phonolite samples have the lowest NBO/T (0.10 and 0.11) related to their higher SiO₂ content. The tephri-phonolite has an intermediate NBO/T of 0.20.

3.2. Viscosity data

The viscosity in air for anhydrous and crystal- and bubble-free basanitic, tephri-phonolitic and phonolitic melts of the Mayotte submarine volcanic chain are presented as a function of temperature in **Figures 3** and **4** and given in **Table 4**. High-temperatures viscosity was obtained for all samples while low-temperature viscosity was only obtained for DR07 (**Fig. 3** and **Table**

4). As discussed below, this is because it was not possible to prepare the crystal-free glass samples needed for the low-temperature measurements for the other samples.

High-temperature viscosity measurements were performed between 1565 K and 1860 K. The lower bond of this range is motivated by the fact that, according to the MELTS model (Ghiorso and Sack 1995), magnetite crystallization is expected to occur below 1450 K for the studied samples. In this restricted high-temperature range, the relationship between viscosity and temperature is mostly linear (Fig. 3), in agreement with Bottinga et al. (1982). The data are therefore interpolated using the Arrhenius relation:

$$\log_{10} \eta = A_{Arr} + \frac{E_a}{RT}, \quad (2)$$

where η is the melt viscosity (Pa·s), A_{Arr} is a constant, T is temperature (K), R is the gas constant (J mol⁻¹ K⁻¹), and E_a is the viscous flow activation energy (kJ mol⁻¹).

For DR07, as we obtained both high- and low-temperatures data (Fig. 3 and Table 4), we use the Vogel-Fulcher-Tamman (VFT; Vogel 1921; Tamman and Hesse 1926; Fulcher 1925) equation to interpolate the viscosity data:

$$\log_{10} \eta = A + \frac{B}{T-C}, \quad (3)$$

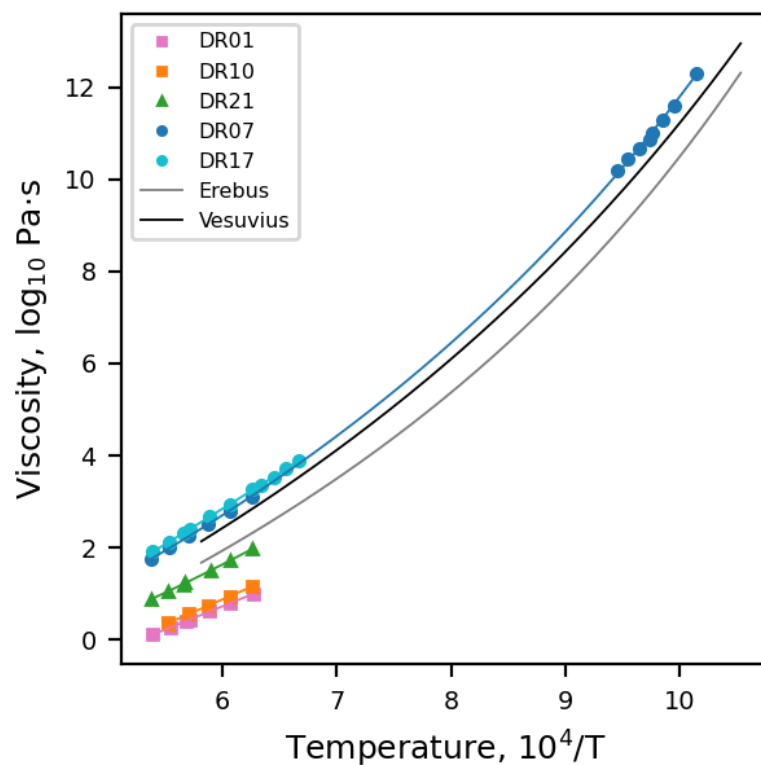
with A , B and C the pre-exponential factor, the pseudo-activation energy and the VFT temperature, respectively. The viscosity-temperature variation of the phonolite melts from Vesuvius and Erebus are also shown as comparison (Fig. 3).

Table 3. Viscosity measurements of the basanitic-to-phonolitic melts along the Mayotte submarine volcanic chain. The uncertainty is equal to or lower than 0.03 log (Pa·s).

| Basanitic melt | | | | Tephri-phonolitic melt | | Phonolitic melt | | | |
|----------------|------------------------------------|------------|------------------------------------|------------------------|------------------------------------|-----------------|------------------------------------|------------|------------------------------------|
| DR01 | | DR10 | | DR21 | | DR07 | | DR17 | |
| T (K) | η (log ₁₀ Pa.s) | T (K) | η (log ₁₀ Pa.s) | T (K) | η (log ₁₀ Pa.s) | T (K) | η (log ₁₀ Pa.s) | T (K) | η (log ₁₀ Pa.s) |
| | | | | | | 986 | 12.30 | | |
| | | | | | | 1006 | 11.61 | | |
| | | | | | | 1016 | 11.30 | | |
| | | | | | | 1025 | 11.00 | | |
| | | | | | | 1027 | 10.87 | | |
| | | | | | | 1037 | 10.67 | | |
| | | | | | | 1048 | 10.44 | | |
| | | | | | | 1058 | 10.19 | | |
| | | | | | | | | 1499 | 3.89 |
| | | | | | | | | 1525 | 3.71 |
| | | | | | | | | 1551 | 3.54 |
| | | | | | | | | 1576 | 3.37 |
| 1595 | 0.99 | 1596 | 1.16 | 1596 | 1.97 | 1597 | 3.10 | 1596 | 3.27 |
| 1646 | 0.79 | 1648 | 0.94 | 1647 | 1.73 | 1648 | 2.80 | 1646 | 2.95 |
| 1698 | 0.61 | 1699 | 0.74 | 1696 | 1.50 | 1700 | 2.52 | 1698 | 2.67 |
| 1749 | 0.43 | 1753 | 0.56 | | | 1751 | 2.25 | 1750 | 2.40 |
| 1761 | 0.40 | | | 1762 | 1.23 | | | | |
| | | | | 1766 | 1.20 | | | 1766 | 2.32 |
| 1801 | 0.27 | 1809 | 0.38 | 1809 | 1.04 | 1804 | 2.01 | 1807 | 2.12 |
| | | 1810 | 0.34 | | | | | | |
| 1855 | 0.11 | | | 1858 | 0.89 | 1860 | 1.75 | 1855 | 1.91 |

At super-liquidus temperatures, the basanitic melts have the lowest viscosity (0.99 to 0.11 log₁₀ Pa·s at 1595 to 1855 K) followed by the tephri-phonolitic (1.97 to 0.89 log₁₀ Pa·s at 1596 to 1858 K) and the phonolitic melts (3.89 to 0.91 log₁₀ Pa·s at 1499 to 1855 K). **Figure 3** shows that, at a given temperature (between 1500 to 1855 K), the viscosity of the basanitic melts differ from those of the phonolitic ones by about two orders of magnitude. In particular, at 1750 K, the viscosity is of 0.43, 1.23 and 2.40 log₁₀ Pa·s, for the basanitic (DR01), tephri-phonolitic (DR21) and phonolitic (DR17) melts, respectively (**Table 3**). At undercooled temperatures, the viscosity of DR07 ranges from 12.3 log₁₀ Pa·s at 986 K to 10.2 log₁₀ Pa·s at 1058 K (**Fig 3**).

311 We compare our measurements to the [Giordano et al. \(2008\)](#) and [Hui and Zhang \(2007\)](#)
 312 empirical models (hereafter abbreviated as the GRD and HZ models, respectively). Based on
 313 **Figure 4**, the GRD model tends to fit well the viscosity of basanite while a slight
 314 underestimation is observable for the tephri-phonolitic melts at high-temperatures. This
 315 becomes critical for the phonolite melts for which the GRD model significantly underestimates
 316 the viscosity at both high- and low-temperatures (**Fig. 4**). Conversely the HZ model tends to
 317 slightly overestimate the viscosity of the basanites and tephri-phonolites at high-temperatures.
 318 It is in good agreement with the measured viscosity of phonolites at high-temperatures but
 319 significantly underestimates the values at low-temperatures (**Fig. 4**). As also shown by [Le Losq](#)
 320 [et al. \(2015a\)](#) the GRD model underestimates by ~ 0.5 log units the viscosity of Erebus (**Fig.**
 321 **4**). In contrast, for the Vesuvius melt, at super-liquidus temperatures there is a difference of
 322 less than almost ~ 0.2 log units between the predicted and the measured viscosity (**Fig. 4A**),
 323 while at low-temperatures the GRD model fits well the viscosity data (**Fig. 4B**).



324

Figure 3. Viscosity ($\log_{10} \text{Pa}\cdot\text{s}$) as a function of inverse temperature (K^{-1}) for the Mayotte basanite-to-phonolite magmatic differentiation trend. Squares, diamonds and circles represent measurements made on basanites (DR01 and DR10), tephri-phonolite (DR21) and phonolites (DR07 and DR17), respectively. Erebus (grey curve) and Vesuvius (black curve) are also represented (data from [Giordano et al. 2009](#); [Le Losq et al. 2015a](#)). Solid lines are interpolations of the data with the VFT equation ([Eq. 3, Table 4](#)). Error bars are smaller than the symbol size.

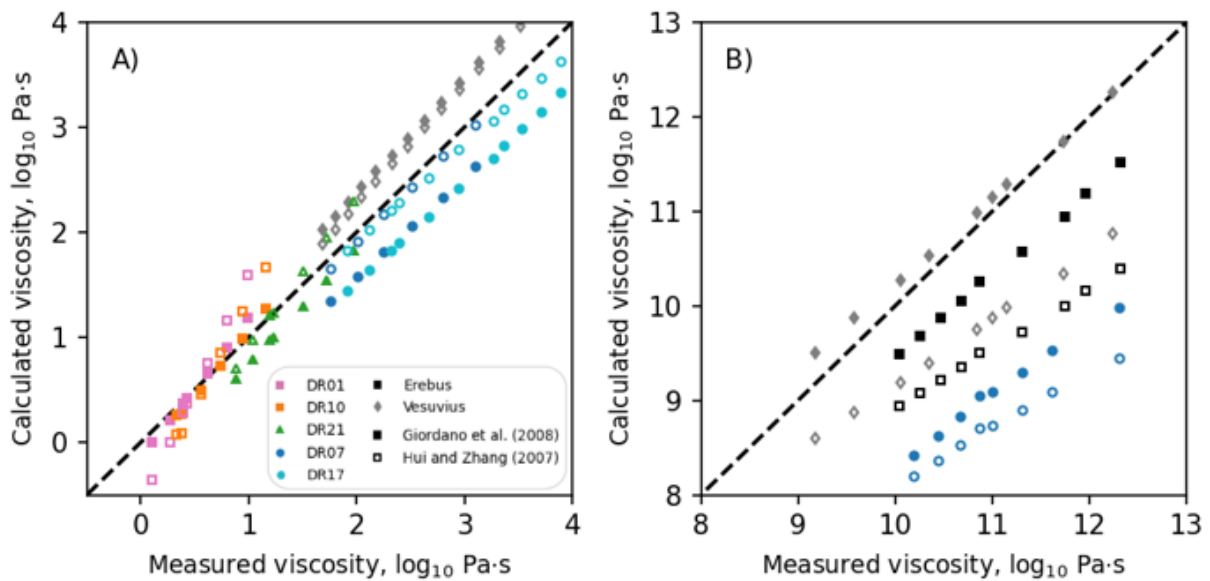


Figure 4. Comparison between the measured viscosity ($\log_{10} \text{Pa}\cdot\text{s}$) and the calculated ones with the models of [Giordano et al. \(2008\)](#) (filled symbols) and of [Hui and Zhang \(2007\)](#) (open symbols) in the super-liquidus (A) and undercooled (B) temperature ranges. Error bars are smaller than the symbol size.

3.3. Raman spectroscopy

To check for crystallization during the low-temperature viscosity experiments, we compare the Raman spectra of DR07 before and after the low-temperature viscosity experiments ([Fig. 5](#)). Before the experiment, the DR07 glass Raman spectrum exhibits three main broad bands near

80, 490 and 1000 cm^{-1} . The first is the Boson peak assigned to transverse acoustic vibrational modes promoted in silicate glasses by cooperative inter-tetrahedral vibrations (Buchenau et al. 1986; Malinovsky and Sokolov 1986; Hehlen et al. 2002). This is a universal signature of the glassy state (Malinovsky and Sokolov 1986), that tends to quickly disappear in the presence of crystals (e.g., Takahashi et al. 2009). The second is the inter-tetrahedral T-O-T (T = Si, Al) vibrations in the aluminosilicate network. The third is assigned to intra-tetrahedral T-O stretching vibration (Mysen et al. 1982; McMillan 1984; Le Losq et al. 2014).

After the low temperature viscometry, the recovered DR07 sample does not show the Boson peak anymore (Fig. 5). This indicates that some degree of crystallization must have occurred during the viscosity measurements near the glass transition.

We also acquired Raman spectra on all the other samples quenched during the initial glass preparation (see supplementary Fig. A1). Although microscopic inspection of the samples appeared crystal-free, and although the Raman spectra above 200 cm^{-1} may not present sharp peaks typical of crystals, no Boson peak was visible. This indicates that initial glass samples other than DR07 contained crystals at a sub-nanometric to nanometric scale (see Discussion). Interestingly, we did not succeed to obtain a pure glass for the DR17 phonolite despite a very similar chemical composition with DR07. This may be explained by the slightly higher Na_2O and Al_2O_3 contents that could be responsible for a different behavior. This testifies that basaltic, tephri-phonolitic and phonolitic crystal-free glass samples of the required size for low temperature viscosimetry are extremely difficult to obtain.

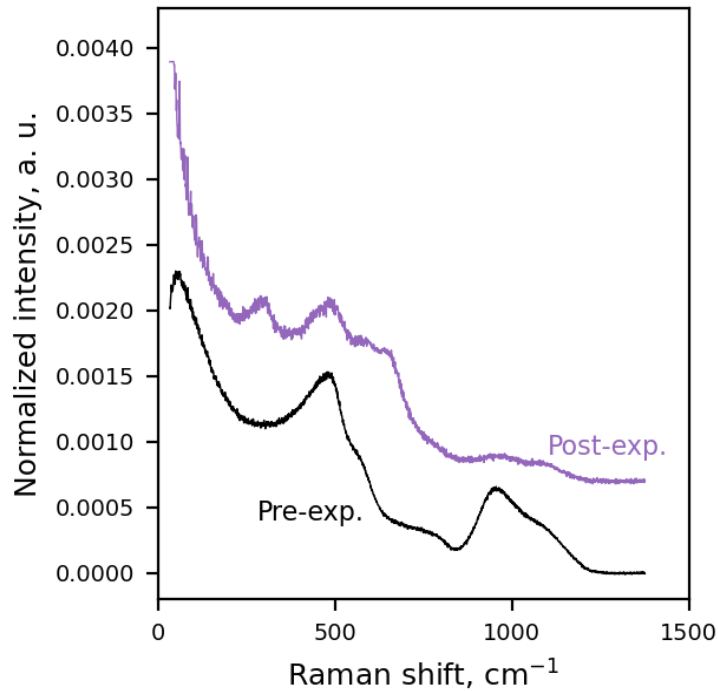


Figure 5. Uncorrected Raman spectra of DR07 phonolite products pre (black curve)- and post (purple curve)-experiments at low-temperature.

4. Discussion

4.1. Nanolite crystallization during low-temperature measurements

DR07 is the only sample for which we obtained a glassy piece large enough to perform near- T_g viscometry. However, during the experiment, the sample seems to have undergone some degree of crystallization as evidenced by the disappearance of the Boson peak (Fig. 5). To confirm that crystallization occurred we acquired a scanning transmission electron microscope (STEM) image with the Helios 5 (ThermoFisher Scientific) scanning electron microscope coupled with a focused ion beam (Xe plasma FIB-SEM) at LMV. Images show the presence of homogeneously distributed brighter particles at the nanoscale (Fig. 6). Similar particles with a size ranging from 5 to 30 nm have been observed and characterized as nanolites (Di Genova et al. 2017, 2018, 2020).

378 The effect of crystallization on viscosity may reach several orders of magnitudes (e.g., [Lejeune](#)
379 [et Richet, 1995](#); [Costa et al. 2009](#); [Mader et al. 2013](#)), particularly in presence of microlites
380 ([Del Gaudio et al. 2013](#)) or nanolites ([Di Genova et al. 2020](#); [Le Losq et al. 2021](#)). In the present
381 case, we observe neither a deviation of the viscosity measurements as a function of time nor
382 the apparition of a non-Newtonian behavior. Therefore, it seems that the presence of nanolites
383 only has limited effects on our measurements. However, this finding suggests that nanolite
384 crystallization happens very quickly in melts of iron-bearing alkaline compositions and even
385 in silica-rich melts such as phonolitic. To check for this, we placed a DR07 glassy sample in
386 an annealing furnace and setup the temperature at the glass transition, with a particular care in
387 avoiding overshooting while checking the sample temperature with a Pt-PtRh10%
388 thermocouple placed in contact with the sample. The Raman spectra of the retrieved sample
389 also showed the presence of crystals in the glass after annealing and is identical to the post-
390 experiment spectra ([Fig. 5](#)). These observations indicate that viscosity measurements for such
391 compositions in the undercooled temperature domain that were presented in previous studies
392 ([Giordano et al. 2000, 2005](#); [Giordano and Dingwell 2003](#); [Le Losq et al. 2015a](#); [Whittington](#)
393 [et al., 2000, 2001](#)) may probably have been also affected by nanolite formation. We add that
394 because diffusion increases with decreasing Si content ([Zhang and Ni 2010](#)), this effect is
395 expected to be even stronger for tephri-phonolitic and basanitic composition, preventing pure
396 glass samples from being obtained. Great care should therefore be taken during low
397 temperature viscometry even for phonolitic melt, and Raman spectra down to the Boson peak
398 wavelength range should be systematically acquired.

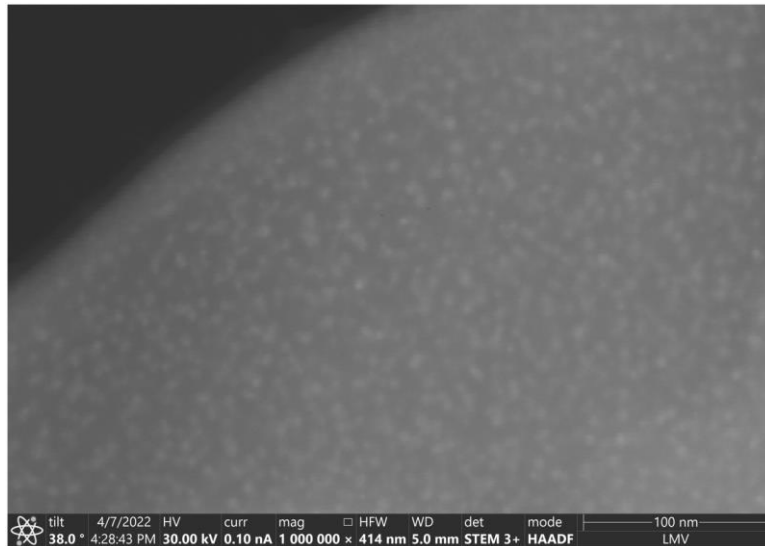


Figure 6. Scanning transmission electron microscope image of the DR07 sample post low-temperatures viscosity measurements.

4.2. Melt viscosity and comparison with models

A discrepancy between experimental measurements and parametric viscosity models, as observed here (**Fig. 4**), has also been previously reported for alkaline composition by [Le Losq et al. \(2015a\)](#). There are two likely causes for the significant difference between the GRD model and the measured viscosity at low temperature. First, unlike at high temperatures, in undercooled melts, important and nonlinear variations in melt configurational entropy result from changes in melt composition and drive important changes in viscosity ([Richet 1984](#); [Neuville and Richet 1991](#); [Le Losq et al. 2021](#)). It is challenging for parametric models to reproduce such strongly nonlinear behavior of viscosity variations and so, this could explain the discrepancy between the GRD model and our low-temperature viscosity measurements. Secondly, the GRD model has been calibrated with a restricted alkaline basanite-to-phonolite compositional data subset ([Giordano et al. 2008](#)). This could reduce the accuracy of the viscosity prediction of this model for such compositions. This also explains why the Vesuvius

melt is better reproduced as this composition was part of the database used to parametrize the GRD model (Giordano et al. 2008).

Additional comparison has been performed between our viscosity measurements and the predictions from the Hui and Zhang (2007) model. The HZ model is in relatively good agreement with our viscosity measurements at high-temperatures (Fig. 4A) whereas it significantly underestimates by $\sim 1.3 \log_{10}$ units the viscosity of phonolitic melts at low-temperatures (Fig. 4B). Similar differences are observed between the HZ model and the measurements made on the Erebus (Le Losq et al. 2015a) and Vesuvius GP79 (Giordano et al. 2009; Le Losq et al. 2015a) samples. According to Hui and Zhang (2007), the model could be improved in part by adding new viscosity measurements at low-temperatures and by considering the effect of ferric and ferrous iron. Also, as for the GRD model, the HZ model is a general model leading to an increase in uncertainty for specific compositions.

In order to refine such pre-existing models and thus improve their accuracy in the viscosity prediction, it is important to keep measuring natural samples. The present viscometry data could then be used to improve such models.

4.3. Polymerization and viscosity

The relationships between the super-liquidus viscosity and melt polymerization, in terms of T-O-T bridging as quantified by the chemically-derived, oxidized NBO/T (Eq. 1), are illustrated in Figure 7. At given temperature, basanite melts show the lowest viscosity ($< 1.2 \log \text{ Pa}\cdot\text{s}$) and the highest NBO/T (0.32 to 0.33) whereas phonolite melts have the highest viscosity ($> 2 \log \text{ Pa}\cdot\text{s}$) and lowest NBO/T (0.10 and 0.11) (Fig. 7). Accordingly, the tephri-phonolite sample, having an intermediate chemical composition (Fig. 2 and Table 2), falls in between the basanite and phonolite compositions (Fig. 7). The fact that the highest viscosity data are obtained for the samples with the lowest NBO/T, and inversely, is an expected pattern (Mysen et al. 1982,

1985; Scarfe et al. 1987; Mysen and Richet 2019). A higher degree of polymerization (lower NBO/T) will lead to lesser solutions for performing the cooperative rearrangements of the molecular sub-units necessary for melt viscous flow. This results, according to the Adam-Gibbs theory of viscous flow, in a lower melt configurational entropy and, hence, in a higher melt viscosity (Adam and Gibbs, 1965; Richet, 1984). Such variations in melt polymerization with composition, albeit expected, may have an important impact on the eruptive style (see Implications).

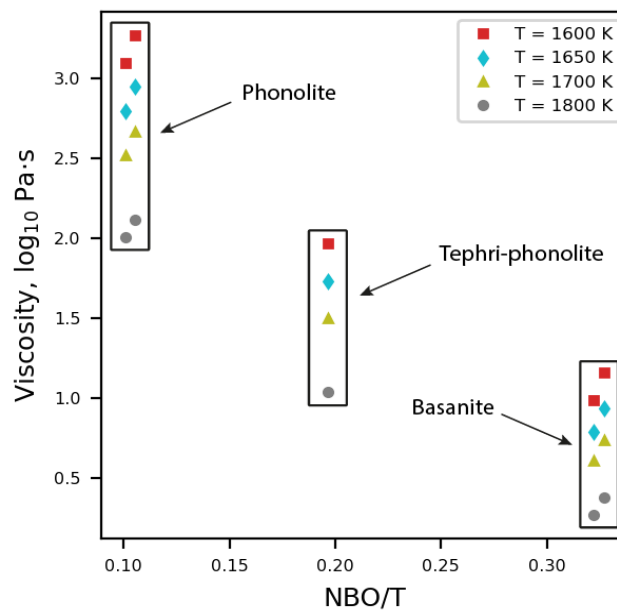


Figure 7. Variations of the viscosity ($\log_{10} \text{Pa}\cdot\text{s}$) at a given temperature relative to composition as represented by the ratio of non-bridging oxygens to tetrahedrally-coordinated cations (NBO/T). See also Table 2 and 3 for chemical compositions and viscosity results, respectively.

4.4. Influence of iron redox state and volatile concentration on melt viscosity

All the presently reported experiments were performed in air. In addition, we measured the viscosity of volatile-free melts, as they degassed upon preparation. Therefore, to provide accurate viscosity estimates of the basanite, tephri-phonolite and phonolite melts in a natural context, we should take into account the influence of both water and iron oxidation state on the

viscosity of the silicate melts. The reduction to Fe^{2+} can lead to a decrease in melt viscosity of 0.2 - 0.5 log units at super-liquidus conditions, which can reach up to 1.5 log units at undercooled temperature conditions (Dingwell and Virgo 1987; Dingwell 1991; Liebske et al. 2003; Drucwrr 2007; Chevrel et al. 2013). Water also strongly participates in lowering the viscosity of alkaline magmas (e.g., Whittington et al., 2000, 2001).

To quantify the effect of water, we here follow the methodology of Le Losq et al. (2015a) who calculated the relative effect of water on the B and C terms of the VFT equation (Eq. 3) for phonolite melts, based on previously published data from Whittington et al. (2001). In that way we use the following equation:

$$\log_{10} \eta = A + (B^{\text{anh}} + K_1 * C_{\text{H}_2\text{O}} + K_2 * C_{\text{H}_2\text{O}}^2) / (T - (C^{\text{anh}} + K_3 * C_{\text{H}_2\text{O}} + K_4 * C_{\text{H}_2\text{O}}^2)), \quad (4)$$

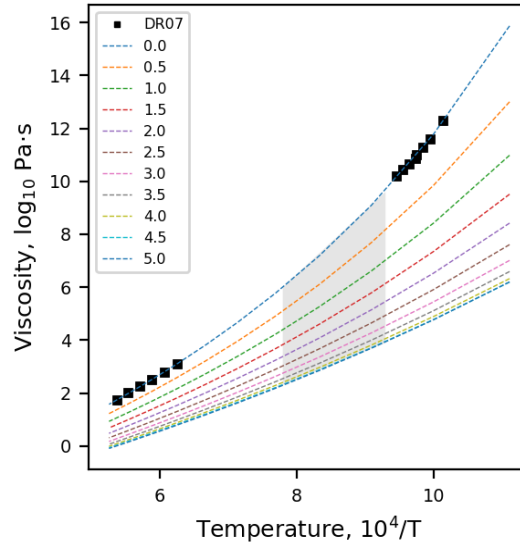
where K_1 , K_2 , K_3 and K_4 are the parameters of the polynomial functions that describe the effect of the water concentration in wt%, $C_{\text{H}_2\text{O}}$, on the value of the parameters B and C. B^{anh} and C^{anh} are the VFT B and C parameters of the anhydrous melt. Regarding the basanite composition no viscosity measurements at undercooled temperatures were obtained for this study. Hence, we calculated the VFT parameters of the anhydrous melt by combining our high-temperature data with the low- temperatures data from Whittington et al. (2000) obtained for an iron-free basanite melt (Table 4). To calculate the K_1 , K_2 , K_3 and K_4 parameters, we then used the VFT parameters published by Whittington et al. (2000) for a hydrous iron-free basanite. Table 5 reports the K_1 , K_2 , K_3 and K_4 parameters from Le Losq et al. (2015a).

Table 4. Parameters obtained for Arrhenius relation at high-temperature (Eq. 2) and VFT parameter over the entire temperature range (Eq. 3). The VFT parameters calculated for the basanite DR10 result from a combination of the high temperatures data from this study and low-temperatures data from Whittington et al. (2000) (see Discussion).

| Sample | Temperature range (K) | Viscosity range (log ₁₀ Pa·s) | A _{Arr} | E _{aArr} (kJ mol ⁻¹) | RMSE _{Arr} | A _{VFT} | B _{VFT} | C _{VFT} | RMSE _{VFT} |
|--------|--------------------------|---|------------------|--|---------------------|------------------|------------------|------------------|---------------------|
| DR01 | 1600 - 1855 | 0.99 - 0.11 | -5.34 | -44.37 | 0.003 | - | - | - | - |
| DR10 | 1600 - 1810 | 1.16 - 0.34 | -5.6 | -46.57 | 0.015 | -3.5 | 4448 | 645 | 0.05 |
| DR21 | 1600 - 1860 | 1.97 - 0.89 | -5.8 | -48.23 | 0.011 | - | - | - | - |
| DR17 | 1500 - 1855 | 3.89 - 1.91 | -6.46 | -53.72 | 0.008 | - | - | - | - |
| DR07 | 990 - 1860 | 12.30 - 1.75 | - | - | - | -3.9 | 7572 | 517 | 0.04 |

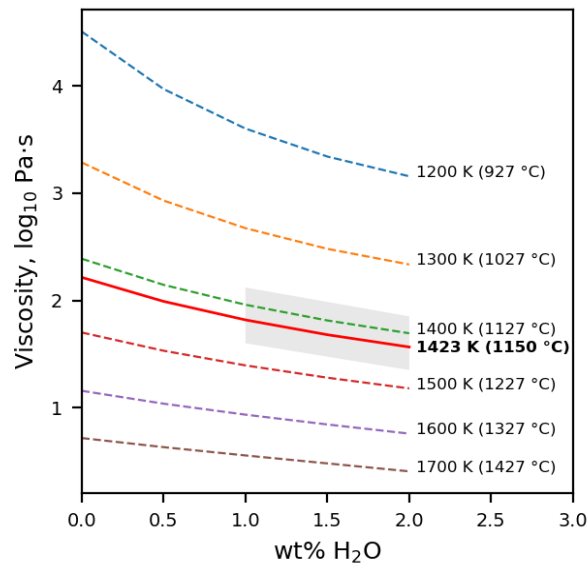
Table 5. K parameters for estimating the effect of water on the parameters B and C of the VFT equation (Eq. 4) for the phonolite (from Le Losq et al. 2015a) and the basanite melts.

| Parameter | Values for phonolite DR07 | Values for basanite melts |
|----------------|---------------------------|---------------------------|
| K ₁ | -455.52 | 403.15 |
| K ₂ | 32.626 | -133.87 |
| K ₃ | -110.61 | -140.77 |
| K ₄ | 13.241 | 32.043 |



494

495 **Figure 8.** Viscosity ($\log_{10} \text{Pa}\cdot\text{s}$) as a function of inverse temperature (K^{-1}) for the DR07
 496 phonolite. Measured viscosity values (squares) are shown together with values predicted
 497 (curves) by **Eq. 4** for different water concentrations (wt %). Numbers in the label refer to water
 498 content in wt% and the expected magmatic conditions are indicated by the grey box. The 4.5
 499 and 5.0 wt% water curves are superposed. Error bars are smaller than the symbol size.



500

501 **Figure 9.** Isothermal viscosity as a function of water concentration (wt%) for the DR10
 502 basanite. The predicted magmatic conditions proposed by [Berthod et al., \(2021b\)](#) are indicated
 503 by the red line (1150 °C) and its uncertainty by the grey box (± 50 °C).

504 We present the effect of water on the phonolite melt (DR07) in **Figure 8** and on the basanite
505 melt (DR10) in **Figure 9**. As expected, the water strongly lowers the viscosity for both melts.
506 The addition of 1 wt% of water reduces the viscosity from 2.50 to 1.68 log₁₀ Pa·s at 1700 K
507 for the DR07 phonolite. The decreasing effect of water on viscosity is higher at lower
508 temperatures, where the difference between anhydrous and hydrous melts may reach up to 4
509 orders of magnitude at 900 K (**Fig. 8**). In contrast, the addition of 1 wt% of water decreases the
510 viscosity of the basanite melt by almost 0.4 log₁₀ units at 1700 K (**Fig. 9**). These results in
511 agreement to those reported by [Whittington et al. \(2000, 2001\)](#). Hence, our results confirm that
512 (i) further addition of water results in a progressively less important decrease in viscosity and
513 (ii) the effect of water is more effective at reducing the viscosity of polymerized melts
514 (phonolites) than for depolymerized melts (basanites). As it has been previously demonstrated,
515 the chemical composition of the melt affects water solution mechanisms, resulting in different
516 effects on melt structure (e.g., [Whittington et al. 2000, 2001](#); [Xue and Kanzaki 2004, 2006](#);
517 [Cody et al. 2005](#); [Mysen and Cody 2005](#); [Mysen and Richet 2005](#); [Giordano et al. 2009](#); [Le](#)
518 [Losq et al. 2015b](#)). For polymerized melts, a common and simple water solution mechanism is
519 the reaction of water molecules with the silicate network, breaking T-O-T bonds (with T = Si,
520 Al) (e.g., see [Mysen and Richet 2019](#); [Le Losq et al. 2015b](#)). In contrast, for depolymerized
521 melts, silicate network and network modifiers (e.g., Ca, Mg) may be implied into the
522 mechanism leading to slight change of the melt polymerization ([Xue and Kanzaki 2004](#);
523 [Moretti et al. 2014](#); [Le Losq et al. 2015b](#)). For the present basanite and phonolite melts that
524 present relatively low NBO/T, the dissolution of water is expected to result in melt
525 depolymerization, but a stronger effect is expected for phonolites as the mechanism implying
526 reaction between T-O-T bonds and water should be more active. This can explain observations
527 made on viscosity (**Figs. 8, 9**).

Thus, the reported values for the viscosity of the silicate melts represent upper limits for aluminosilicate melts due to the effect of water combined with the iron oxidation state.

4.5. Comparison of phonolites viscosities from different areas

We can compare the viscosity of the phonolites from Mayotte (DR07 and DR17) to data from previous studies on similar Al- and alkali-rich compositions. For this, the viscosity measurements of the phonolitic Erebus (Le Losq et al. 2015a) and Vesuvius GP79 (Giordano et al. 2009; Le Losq et al. 2015a) magmatic melts have been selected (Fig. 3). The viscosity of the Vesuvius GP79 sample is lower by an order of magnitude compared to the phonolite from the East-Mayotte submarine volcanic chain. This may be explained by a lower SiO₂ content (54 wt% against 59 wt%). Despite a similar composition in SiO₂ and alkali elements (Fig. 2 and Table 2), the viscosity of DR07 differs from the Erebus one by about 0.5 orders of magnitude. The phonolites of Mayotte (DR07 and DR17) are richer by 1 to 2 wt% of iron compared to the Erebus sample (Table 2). In contrast to Chevrel et al. (2013), a decrease in melt viscosity with increasing iron concentration is not observed. The observed viscosity difference more probably finds its origin in variations in the concentrations of a few elements such as K, Mg and Ca between the phonolites of Mayotte and Erebus. Indeed, the DR07 and DR17 samples are slightly more enriched in K₂O (Table 2). In aluminosilicate compositions, addition of K₂O can lead to decreasing the melt configurational entropy and so, to increasing its viscosity at constant temperature (Le Losq et al. 2013, 2017, 2021; Robert et al. 2019). Therefore, the difference in K₂O between the Erebus and Mayotte phonolites could explain the observed viscosity distinctions. In addition, the Erebus sample contains a bit more alkaline-earth elements (Mg and Ca), that may act as *network modifiers* and favor the creation of non-bridging oxygen (NBO) atoms and, hence, a decrease in viscosity (Mysen et al. 1980; Mysen 1995; Richet et al. 1984; Stebbins et al. 1992; Stebbins and Xu 1997). Hence, it seems

consistent that the DR07 phonolite from Mayotte has a higher viscosity than the Erebus sample. As explained previously, no viscosity measurements at undercooled temperatures could be obtained for the DR17 phonolite. However, according to the viscosity at the super-liquidus temperatures and the enrichment in alkali (**Figs. 2 and 3**) we may assume that the viscosity at undercooled temperatures will be higher than the DR07, Erebus and Vesuvius melts.

5. Implication on eruption dynamics

Upon magma ascent in a conduit, the style of a volcanic eruption depends on whether the magma fragmentation threshold is crossed (explosive) or not (effusive). This threshold will depend on the magma viscosity but also on the ascending rate and bubble overpressure (e.g., [Dingwell et al. 1996](#); [Papale 1999](#); [Ma et al. 1999](#); [Pistolesi et al. 2011](#); [Gonnermann et al. 2011](#); [Gonnermann 2015](#)). Generally, in magmas with high viscosity (silica-rich composition), the enhanced resistance to bubble expansion favors bubble overpressure and reduces the ability of volatiles to stream out of the melt. This in turn promotes more efficient magma fragmentation and a greater explosivity of eruptions. Of course, many exceptions break such general rules, such as basaltic Plinian eruptions (e.g., [Moitra et al. 2018](#)) and Si-rich lava flows (e.g., [Fink 1983](#); [Farquharson et al. 2015](#); [Prival 2021](#)). Additionally, eruption style can switch between effusive and explosive activities during an eruption due to variations in magma composition, degassing, and crystallization that all drive magma viscosity (e.g., Vesuvius [Giordano et al. 2009](#); [Myers et al. 2021](#), [Andújar and Scaillet 2012](#); [Popa et al. 2021](#)). Attempts have been done to define the viscosity threshold to discriminate explosive to effusive eruptions, but no consensus has yet been achieved ([Papale 1999](#); [Di Genova et al. 2017](#); [Wadsworth et al. 2018](#)).

Our results show that basanite melts have the lowest viscosity of the series followed by the tephri-phonolite and the phonolite melts and that the presence of water reduces the viscosity.

578 Assuming that the eruptive temperature (T_e) of the Mont Fani Maoré basanite lavas is around
579 1150 °C (Berthod et al., 2021b), and that water content could range from 1.0 to 2.3 wt%
580 (Berthod et al. 2021b), we thus expect lava viscosity upon eruption to range from 1.5 to 2.5
581 \log_{10} Pa·s (Fig. 8). Such a viscosity range is close to, for example, the viscosity of subaerial
582 pahoehoe basaltic lavas from Hawaii (Chevrel et al. 2018) or submarine basaltic lava flows
583 (McClinton et al. 2014). This low viscosity range is therefore consistent with the effusive
584 eruption style and morphologies (pillow lavas and pahoehoe lavas) of the lava flow field as
585 observed at Mont Fani Maoré (Feuillet et al., 2021; Berthod et al. 2021b). However, several
586 questions remain. Why did the basanite melt come out from the Mont Fani Maoré rather than
587 ascend upwards to erupt in the Horseshoe site, where its hypothesized magmatic storage is
588 located (Lemoine et al. 2020; Feuillet et al. 2021)? Does the low viscosity of the basanite melt
589 favored a lateral pathway? Could the low viscosity favors high flux rates ($150 - 200 \text{ m}^3 \text{ s}^{-1}$
590 averaged over the first year, Berthod et al. 2021b) and the long duration eruption if the volume
591 was there?

592 Around the Horseshoe volcanic site of the Mayotte volcanic chain, a large diversity of edifice
593 morphologies and deposits textures corresponding to both phonolitic effusive and explosive
594 eruptions have been observed (REVOSIMA, 2022; Puzenat et al. 2022; Gurioli et al. 2023;
595 Komorowski et al. 2023). Such diversity can be explained by the fact that, depending on magma
596 ascent rates, eruptive temperatures and initial water contents, phonolite magmas can be
597 involved in a broad range of magmatic effusive and explosive activity (e.g., see Andújar and
598 Scaillet 2012). Indeed, the Mayotte phonolite magmas evolved from basanite magma by ~80%
599 of fractional crystallization (Berthod et al. 2021a). They are expected to present a high viscosity
600 at expected eruption temperatures (typically in the 800-1000 °C range, e.g. see Andújar and
601 Scaillet 2012). However, phonolite magmas are also expected to contain a large amount of
602 dissolved water. If assuming a phonolite melt stored in a deep magma chamber at $T_e = 800 -$

1000 °C and containing ~5 wt% water (Andújar and Scaillet 2012), this magma could have a viscosity as low as 2.0 - 3.2 log₁₀ Pa·s (Fig. 8), not that far from that previously estimated for the basanite melt. However, upon migration toward the surface, vigorous water exsolution is expected to occur. According to the composition of the residual glass of the submarine phonolites from Mayotte (encountered at 1,300 to 1,600 m b.s.l.), the residual water content in erupted phonolite glass ranges between 0.8 and 1.2 wt% (Thivet, personal communication). Considering such values, the viscosity of the phonolite melts may increase of up to 4 to 7 orders of magnitudes upon ascent (Fig. 8). In parallel, the significant water exsolution will lead to the formation of a magmatic foam of low density in the conduit, reinforcing the buoyant force that pushes the magma out toward surface. This effect is particularly promoted in silica-rich melts like phonolites, because their high viscosity favors entrapment of the bubbles (Thomas et al. 1994; Gardner et al. 1996). Therefore, exsolution of water from such magmatic liquids often results in foaming, largely enhancing the probability of brittle fragmentation of the foam (Jones et al. 2019; Scheu and Dingwell 2022) in the conduit (e.g., Dingwell, 1996; Papale 1999; Gonnerman, 2015). Therefore, the amount of water initially stored in the chambers will determine the eruptive styles. The occurrence of both effusive and explosive phonolite eruptions at Mayotte, testified by the observed deposits and products, indicate that a broad range of storage conditions and degassing history exist along this volcanic chain, leading to open questions regarding the future events that could imply phonolite melts.

6. Conclusion

This study provides precise quantification of the temperature-viscosity relationship for basanite to phonolite melts through a large temperature range and discusses the effect of dissolved water on melt viscosity. We show that at eruption temperatures basanite lavas are more propitious to erupt in an effusive manner while phonolite may erupt effusively or explosively. However, we

do not account for the effect of bubbles and crystals on magma viscosity. Future studies should accounted for their effect to provide a holistic view of magma rheology which directly impacts the dynamics and eruption style as well as lava flow emplacement. For this, detailed sample texture analyses should be undertaken on collected samples to quantify the bubble and crystal content, shape, size and distribution that are necessary to constrain magma suspension rheology (see [Harris and Allen 2008](#); [Mader et al. 2013](#); [Kolzenburg et al. 2022](#)). Measuring the viscosity of magmatic liquids along the Mayotte alkali magmatic differentiation trend combined with known volatile content, and crystal and bubbles characteristics, is essential to quantify the evolution of magma viscosity during ascent rate, outgassing and crystallization, which directly influence the prevailing conditions determining the eruptive style (whether it is effusive or explosive).

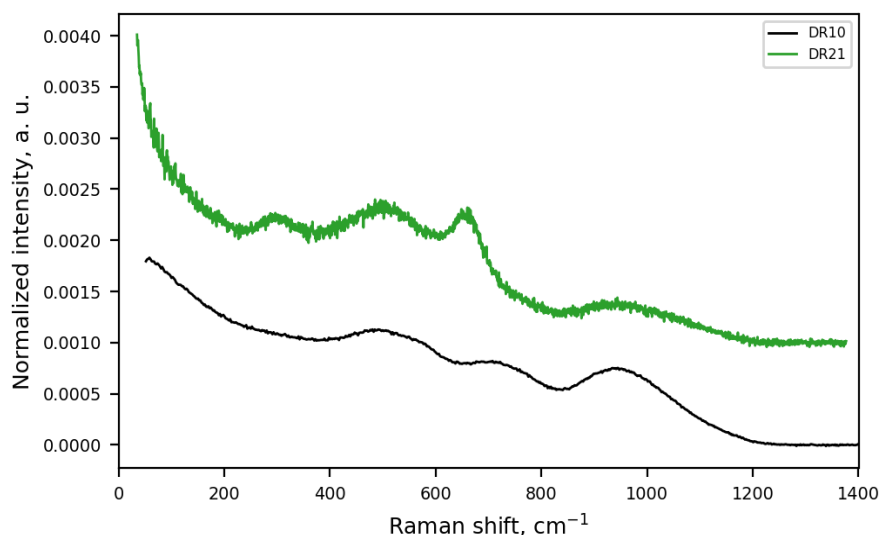
Acknowledgments

MAYOBS 1 campaign was funded by the CNRS-INSU TELLUS MAYOTTE program (SISMAYOTTE project). MAYOBS 1, 2, 4 and 15 campaigns were conducted by several French research institutions and laboratories (IPGP/CNRS/BRGM/IFREMER/IPGS). All marine operations are performed as part of the MAYOBS set of campaigns (<https://doi.org/10.18142/291>) and we thank the captains and crews of the R/V Marion Dufresne (TAAF/IFREMER/LDA), R/V *Pourquoi Pas?* (GENAVIR/IFREMER, SHOM). We thank the mission chiefs of the MAYOBS campaigns (E. Rinnert, N. Feuillet, Y. Fouquet, S. Jorry, I. Thinon, E. Lebas, F. Paquet) and of the GeoFlamme oceanographic campaign (CNFH; PI C. Cathalot, E. Rinnert, N. Feuillet) for conducting marine operations that benefited this study and provided dredge samples. We also thank additional scientists on board the MAYOBS cruises that conducted the dredge operations and processed the samples (P. Besson, M. Bickert, P. Burckel, B. Caron, C. Deplus, S. Hidalgo, A. Le Friant, S. Nowak). We thank A. Peltier (OVPF-

IPGP) and C. Mucig (BRGM Mayotte) respectively the Operational Leader and Co-leader of the REVOSIMA. We thank the scientists of REVOSIMA consortium for access to data and for discussions during the Scientific and Technical Committee meetings. Analyses were funded by the Service National d'Observation en Volcanologie (SNOV, INSU) and the Réseau de Surveillance Volcanologique et Sismologique de Mayotte (REVOSIMA), a partnership between the Institut de Physique du Globe de Paris (IPGP), the Bureau de Recherches Géologiques et Minières (BRGM), and the Observatoire Volcanologique du Piton de la Fournaise (OVPF-IPGP), the Centre National de la Recherche Scientifique (CNRS), and the Institut Français de Recherche pour l'Exploitation de la Mer (IFREMER). Since June 2019, all activities on Mayotte are funded by le ministère de l'Enseignement Supérieur, de la Recherche et de l'Innovation (MESRI), le Ministère de la Transition Ecologique (MTE), le Ministère des Outremers (MOM), le Ministère de l'Intérieur (MI), and le Ministère des Armées with the support of the DIRMOM (Direction Interministérielle aux Risques Majeurs en Outremer) and the MAPPPROM (Mission d'appui aux politiques publiques pour la prévention des risques majeurs en Outremer). We thank the IPGP for general funding to the Observatoires Volcanologiques et Sismologiques (OVS). The data contributes to the Service National d'Observation en Volcanologie (SNOV). The authors would like to thank IFREMER for their welcome during the sampling and E. Humler for his support and national funding coordination (CNRS, REVOSIMA). The authors also thank Thivet S. for the discussion about the water content within the submarine volcanic samples from Mayotte. Raman and viscosity measurements were supported *in kind* by funds from the IPGP Geomaterial group. This work contributes to IdEx Université de Paris ANR-18-IDEX-0001. This project has received funding from the Institut de Recherche pour le Développement (IRD) and the French Government Laboratory of Excellence initiative no. ANR-10-LABX-0006. This is **Laboratory of Excellence ClerVolc contribution n° X.**

Appendix

Figure A1. Uncorrected Raman spectra of (a.) DR01 basanite (black curve) and (b.) DR21 tephri-phonolite (green curve) products. No Raman Boson peaks are observed on these samples between 50 and 80 cm^{-1} .



682

References Cited

- 684 Adam, G., Gibbs, J.H., 1965. On the Temperature Dependence of Cooperative Relaxation
685 Properties in Glass-Forming Liquids. J. Chem. Phys. 43, 139–146.
686 <https://doi.org/10.1063/1.1696442>
- 687 Andújar, J., Scaillet, B., 2012. Relationships between pre-eruptive conditions and eruptive
688 styles of phonolite–trachyte magmas. Lithos 152, 122–131.
689 <https://doi.org/10.1016/j.lithos.2012.05.009>
- 690 Bachèlery, P., Hémond, C., 2016. Geochemical and Petrological Aspects of Karthala Volcano,
691 in: Bachelery, P., Lenat, J.-F., Di Muro, A., Michon, L. (Eds.), Active Volcanoes of the
692 Southwest Indian Ocean, Active Volcanoes of the World. Springer Berlin Heidelberg,
693 Berlin, Heidelberg, pp. 367–384. https://doi.org/10.1007/978-3-642-31395-0_23
- 694 Bachelery, P., Lenat, J.-F., Di Muro, A., Michon, L. (Eds.), 2016. Active Volcanoes of the
695 Southwest Indian Ocean: Piton de la Fournaise and Karthala, Active Volcanoes of the
696 World. Springer Berlin Heidelberg, Berlin, Heidelberg. [https://doi.org/10.1007/978-3-](https://doi.org/10.1007/978-3-642-31395-0)
697 642-31395-0
- 698 Behrens, H., Roux, J., Neuville, D.R., Siemann, M., 2006. Quantification of dissolved H₂O in
699 silicate glasses using confocal microRaman spectroscopy. Chem. Geol. 229, 96–112.
700 <https://doi.org/10.1016/j.chemgeo.2006.01.014>

- 701 Berthod, C., Médard, E., Bachèlery, P., Gurioli, L., Di Muro, A., Peltier, A., Komorowski, J.-
702 C., Benbakkar, M., Devidal, J.-L., Langlade, J., Besson, P., Boudon, G., Rose-Koga,
703 E., Deplus, C., Le Friant, A., Bickert, M., Nowak, S., Thinon, I., Burckel, P., Hidalgo,
704 S., Kaliwoda, M., Jorry, S.J., Fouquet, Y., Feuillet, N., 2021a. The 2018-ongoing
705 Mayotte submarine eruption: Magma migration imaged by petrological monitoring.
706 *Earth Planet. Sci. Lett.* 571, 117085. <https://doi.org/10.1016/j.epsl.2021.117085>
- 707 Berthod, C., Médard, E., Di Muro, A., Hassen Ali, T., Gurioli, L., Chauvel, C., Komorowski,
708 J.-C., Bachèlery, P., Peltier, A., Benbakkar, M., Devidal, J.-L., Besson, P., Le Friant,
709 A., Deplus, C., Nowak, S., Thinon, I., Burckel, P., Hidalgo, S., Feuillet, N., Jorry, S.,
710 Fouquet, Y., 2021b. Mantle xenolith-bearing phonolites and basanites feed the active
711 volcanic ridge of Mayotte (Comoros archipelago, SW Indian Ocean). *Contrib. Mineral.*
712 *Petrol.* 176, 75. <https://doi.org/10.1007/s00410-021-01833-1>
- 713 Berthod, C., Komorowski, J.-C., Gurioli, L., Médard, E., Bachèlery, P., Besson, P., Verdurme,
714 P., Chevrel, O., Di Muro, A., Peltier, A., and others (2022) Temporal magmatic
715 evolution of the Fani Maoré submarine eruption 50 km east of Mayotte revealed by in
716 situ sampling and petrological monitoring. **Submitted to *Comptes Rendus***
717 ***Geoscience*, Special issue.**
- 718 Bottinga, Y., Weill, D., Richet, P., 1982. Density calculations for silicate liquids. I. Revised
719 method for aluminosilicate compositions. *Geochim. Cosmochim. Acta* 46, 909–919.
720 [https://doi.org/10.1016/0016-7037\(82\)90047-3](https://doi.org/10.1016/0016-7037(82)90047-3)
- 721 Bottinga, Y., Weill, D.F., 1972. The viscosity of magmatic silicate liquids; a model calculation.
722 *Am. J. Sci.* 272, 438–475. <https://doi.org/10.2475/ajs.272.5.438>
- 723 Bouhifd, M.A., Richet, P., Besson, P., Roskosz, M., Ingrin, J., 2004. Redox state,
724 microstructure and viscosity of a partially crystallized basalt melt. *Earth Planet. Sci.*
725 *Lett.* 218, 31–44. [https://doi.org/10.1016/S0012-821X\(03\)00641-1](https://doi.org/10.1016/S0012-821X(03)00641-1)
- 726 Buchenau, U., Prager, M., Nücker, N., Dianoux, A.J., Ahmad, N., Phillips, W.A., 1986. Low-
727 frequency modes in vitreous silica. *Phys. Rev. B* 34, 5665–5673.
728 <https://doi.org/10.1103/PhysRevB.34.5665>
- 729 Castro, J., Walter, S., 2021. Hybrid rhyolitic eruption at Big Glass Mountain, CA, USA.
730 *Volcanica* 4, 257–277. <https://doi.org/10.30909/vol.04.02.257277>
- 731 Cesca, S., Letort, J., Razafindrakoto, H.N.T., Heimann, S., Rivalta, E., Isken, M.P., Nikkhoo,
732 M., Passarelli, L., Petersen, G.M., Cotton, F., Dahm, T., 2020. Drainage of a deep
733 magma reservoir near Mayotte inferred from seismicity and deformation. *Nat. Geosci.*
734 13, 87–93. <https://doi.org/10.1038/s41561-019-0505-5>
- 735 Chevrel, M.O., Baratoux, D., Hess, K.-U., Dingwell, D.B., 2014. Viscous flow behavior of
736 tholeiitic and alkaline Fe-rich martian basalts. *Geochim. Cosmochim. Acta* 124, 348–
737 365. <https://doi.org/10.1016/j.gca.2013.08.026>
- 738 Chevrel, M.O., Harris, A.J.L., James, M.R., Calabrò, L., Gurioli, L., Pinkerton, H., 2018. The
739 viscosity of pāhoehoe lava: In situ syn-eruptive measurements from Kilauea, Hawaii.
740 *Earth Planet. Sci. Lett.* 493, 161–171. <https://doi.org/10.1016/j.epsl.2018.04.028>

741 Chevrel, M.O., Platz, T., Hauber, E., Baratoux, D., Lavallée, Y., Dingwell, D.B., 2013. Lava
 742 flow rheology: A comparison of morphological and petrological methods. *Earth Planet.*
 743 *Sci. Lett.* 384, 109–120. <https://doi.org/10.1016/j.epsl.2013.09.022>

744 Cioni, R., Sbrana, A., Gurioli, L., 1998. The AD 79 Plinian “Pompei” eruption.

745 Cody, G.D., Mysen, B.O., Lee, S.K., 2005. Structure vs. composition: A solid-state ^1H and
 746 ^{29}Si NMR study of quenched glasses along the Na_2O - SiO_2 - H_2O join. *Geochim.*
 747 *Cosmochim. Acta* 69, 2373–2384. <https://doi.org/10.1016/j.gca.2004.11.012>

748 Costa, A., Caricchi, L., Bagdassarov, N., 2009. A model for the rheology of particle-bearing
 749 suspensions and partially molten rocks: RHEOLOGY OF PARTICLE-BEARING
 750 SUSPENSIONS. *Geochim. Geophys. Geosystems* 10, n/a-n/a.
 751 <https://doi.org/10.1029/2008GC002138>

752 Couette, M., 1890. *Etudes sur le frottement des liquides.*

753 Del Gaudio, P., Ventura, G., Taddeucci, J., 2013. The effect of particle size on the rheology of
 754 liquid-solid mixtures with application to lava flows: Results from analogue
 755 experiments: Rheology of Liquid-Solid Mixtures. *Geochim. Geophys. Geosystems* 14,
 756 2661–2669. <https://doi.org/10.1002/ggge.20172>

757 Di Genova, D.D., Caracciolo, A., Kolzenburg, S., 2018. Measuring the degree of
 758 “nanotilization” of volcanic glasses: Understanding syn-eruptive processes recorded in
 759 melt inclusions. *Lithos* 318–319, 209–218. <https://doi.org/10.1016/j.lithos.2018.08.011>

760 Di Genova, D.D., Sicola, S., Romano, C., Vona, A., Fanara, S., Spina, L., 2017. Effect of iron
 761 and nanolites on Raman spectra of volcanic glasses: A reassessment of existing
 762 strategies to estimate the water content. *Chem. Geol.* 475, 76–86.
 763 <https://doi.org/10.1016/j.chemgeo.2017.10.035>

764 Di Genova, D., Zandona, A., Deubener, J., 2020. Unravelling the effect of nano-heterogeneity
 765 on the viscosity of silicate melts: Implications for glass manufacturing and volcanic
 766 eruptions. *J. Non-Cryst. Solids* 545, 120248.
 767 <https://doi.org/10.1016/j.jnoncrysol.2020.120248>

768 Dingwell, D.B., 1991. Redox viscometry of some Fe-bearing silicate melts. *Am. Mineral.* 76,
 769 1560–1562.

770 Dingwell, D.B., 1986. Viscosity-temperature relationships in the system $\text{Na}_2\text{Si}_2\text{O}_5$ -
 771 $\text{Na}_4\text{Al}_2\text{O}_5$. *Geochim. Cosmochim. Acta* 50, 1261–1265. [https://doi.org/10.1016/0016-7037\(86\)90409-6](https://doi.org/10.1016/0016-7037(86)90409-6)

772

773 Dingwell, D.B., Romano, C., Hess, K.-U., 1996. The effect of water on the viscosity of a
 774 haplogranitic melt under P-T-X conditions relevant to silicic volcanism. *Contrib.*
 775 *Mineral. Petrol.* 124, 19–28. <https://doi.org/10.1007/s004100050170>

776 Dingwell, D.B., Virgo, D., 1987. The effect of oxidation state on the viscosity of melts in the
 777 system Na_2O - FeO - Fe_2O_3 - SiO_2 . *Geochim. Cosmochim. Acta* 51, 195–205.
 778 [https://doi.org/10.1016/0016-7037\(87\)90231-6](https://doi.org/10.1016/0016-7037(87)90231-6)

779 Drucwrr, D.B., 2007. Redox viscometry of some Fe-bearing silicate melts.

780 Emmanuel, R., Isabelle, T., Elodie, L., 2021. MAYOBS21 cruise, Marion Dufresne R/V.
781 <https://doi.org/10.17600/18001986>

782 Emmanuel, R., Isabelle, T., FEUILLET Nathalie, 2020. MD 228 / MAYOBS15 cruise, Marion
783 Dufresne R/V. <https://doi.org/10.17600/18001745>

784 Farquharson, J.I., James, M.R., Tuffen, H., 2015. Examining rhyolite lava flow dynamics
785 through photo-based 3D reconstructions of the 2011–2012 lava flowfield at Cordón-
786 Caulle, Chile. *J. Volcanol. Geotherm. Res.* 304, 336–348.
787 <https://doi.org/10.1016/j.jvolgeores.2015.09.004>

788 Feuillet, N., Jorry, S., Crawford, W.C., Deplus, C., Thinon, I., Jacques, E., Saurel, J.M.,
789 Lemoine, A., Paquet, F., Satriano, C., Aiken, C., Foix, O., Kowalski, P., Laurent, A.,
790 Rinnert, E., Cathalot, C., Donval, J.-P., Guyader, V., Gaillot, A., Scalabrin, C., Moreira,
791 M., Peltier, A., Beauducel, F., Grandin, R., Ballu, V., Daniel, R., Pelleau, P., Gomez,
792 J., Besançon, S., Geli, L., Bernard, P., Bachelery, P., Fouquet, Y., Bertil, D.,
793 Lemarchand, A., Van der Woerd, J., 2021. Birth of a large volcanic edifice offshore
794 Mayotte via lithosphere-scale dyke intrusion. *Nat. Geosci.*
795 <https://doi.org/10.1038/s41561-021-00809-x>

796 Feuillet N., 2019. MAYOBS1 cruise, Marion Dufresne R/V.
797 <https://doi.org/10.17600/18001217>

798 Fink, J.H., 1983. Structure and emplacement of a rhyolitic obsidian flow: Little Glass
799 Mountain, Medicine Lake Highland, northern California. *Geol. Soc. Am. Bull.* 94, 362.
800 [https://doi.org/10.1130/0016-7606\(1983\)94<362:SAEOAR>2.0.CO;2](https://doi.org/10.1130/0016-7606(1983)94<362:SAEOAR>2.0.CO;2)

801 Fouquet Y., Feuillet N., 2019. MAYOBS4 cruise, Marion Dufresne R/V.
802 <https://doi.org/10.17600/18001238>

803 Fulcher, G.S., 1925. ANALYSIS OF RECENT MEASUREMENTS OF THE VISCOSITY OF
804 GLASSES. *J. Am. Ceram. Soc.* 8, 339–355. <https://doi.org/10.1111/j.1151-2916.1925.tb16731.x>

806 Gardner, J.E., Thomas, R.M.E., Jaupart, C., Tait, S., 1996. Fragmentation of magma during
807 Plinian volcanic eruptions. *Bull. Volcanol.* 58, 144–162.
808 <https://doi.org/10.1007/s004450050132>

809 Ghiorso, M.S., Sack, R.O., 1995. Chemical mass transfer in magmatic processes IV. A revised
810 and internally consistent thermodynamic model for the interpolation and extrapolation
811 of liquid-solid equilibria in magmatic systems at elevated temperatures and pressures.
812 *Contrib. Mineral. Petrol.* 119, 197–212. <https://doi.org/10.1007/BF00307281>

813 Giordano, D., Ardia, P., Romano, C., Dingwell, D.B., Di Muro, A., Schmidt, M.W.,
814 Mangiacapra, A., Hess, K.-U., 2009. The rheological evolution of alkaline Vesuvius
815 magmas and comparison with alkaline series from the Phlegrean Fields, Etna,
816 Stromboli and Teide. *Geochim. Cosmochim. Acta* 73, 6613–6630.
817 <https://doi.org/10.1016/j.gca.2009.07.033>

818 Giordano, D., Dingwell, D., 2003. Viscosity of hydrous Etna basalt: implications for Plinian-
819 style basaltic eruptions. *Bull. Volcanol.* 65, 8–14. [https://doi.org/10.1007/s00445-002-](https://doi.org/10.1007/s00445-002-0233-2)
820 0233-2

821 Giordano, D., Dingwell, D.B., Romano, C., 2000. Viscosity of a Teide phonolite in the welding
822 interval. *J. Volcanol. Geotherm. Res.* 103, 239–245. [https://doi.org/10.1016/S0377-](https://doi.org/10.1016/S0377-0273(00)00226-2)
823 0273(00)00226-2

824 Giordano, D., Nichols, A.R.L., Dingwell, D.B., 2005. Glass transition temperatures of natural
825 hydrous melts: a relationship with shear viscosity and implications for the welding
826 process. *J. Volcanol. Geotherm. Res.* 142, 105–118.
827 <https://doi.org/10.1016/j.jvolgeores.2004.10.015>

828 Giordano, D., Russell, J.K., Dingwell, D.B., 2008. Viscosity of magmatic liquids: A model.
829 *Earth Planet. Sci. Lett.* 271, 123–134. <https://doi.org/10.1016/j.epsl.2008.03.038>

830 Gonnermann, H.M., 2015. Magma Fragmentation. *Annu. Rev. Earth Planet. Sci.* 43, 431–458.
831 <https://doi.org/10.1146/annurev-earth-060614-105206>

832 Gonnermann, H.M., Houghton, B.F., Adams, N.K., Hildreth, E.W., 2011. The effect of CO₂ on
833 magma vesiculation during explosive volcanic eruptions, in: AGU Fall Meeting
834 Abstracts. pp. V23H-06.

835 Gurioli L., Komorowski J-C., Berthod C., Médard E., Lacombe T., Verdurme P., Bachèlery P.,
836 Mitra S., Falvard S., Paris R. and others (2023) Anatomy of a submarine past volcanic
837 explosion east Mayotte: quantification of primary fragmentation. IAVCEI Scientific
838 Assembly, Rotorua, New-Zealand.

839 Harris, A.J.L., Allen, J.S., 2008. One-, two- and three-phase viscosity treatments for basaltic
840 lava flows. *J. Geophys. Res.* 113, B09212. <https://doi.org/10.1029/2007JB005035>

841 Hehlen, B., Courtens, E., Yamanaka, A., Inoue, K., 2002. Nature of the Boson peak of silica
842 glasses from hyper-Raman scattering. *J. Non-Cryst. Solids* 307, 87–91.

843 Hui, H., Zhang, Y., 2007. Toward a general viscosity equation for natural anhydrous and
844 hydrous silicate melts. *Geochim. Cosmochim. Acta* 71, 403–416.
845 <https://doi.org/10.1016/j.gca.2006.09.003>

846 Jones, T.J., Reynolds, C.D., Boothroyd, S.C., 2019. Fluid dynamic induced break-up during
847 volcanic eruptions. *Nat. Commun.* 10, 3828. [https://doi.org/10.1038/s41467-019-](https://doi.org/10.1038/s41467-019-11750-4)
848 11750-4

849 Jorry S., J., 2019. MAYOBS2 cruise, Marion Dufresne R/V.
850 <https://doi.org/10.17600/18001222>

851 Kelly, P.J., Kyle, P.R., Dunbar, N.W., Sims, K.W.W., 2008. Geochemistry and mineralogy of
852 the phonolite lava lake, Erebus volcano, Antarctica: 1972–2004 and comparison with
853 older lavas. *J. Volcanol. Geotherm. Res.* 177, 589–605.
854 <https://doi.org/10.1016/j.jvolgeores.2007.11.025>

855 Kolzenburg, S., Chevrel, M.O., Dingwell, D.B., 2022. Magma / Suspension Rheology. *Rev.*
856 *Mineral. Geochem.* 87, 639–720. <https://doi.org/10.2138/rmg.2022.87.14>

- 857 Komorowski J-C., Gurioli L., Berthod C., Médard E., Verdurme P., Puzenat V., Bachèlery P.,
858 Chevrel O., Paquet F., Lebas E. and others (2023) The submarine monogenetic volcanic
859 field East of Mayotte (France, Indian Ocean): an exceptional diversity of effusive and
860 explosive processes revealed by recurrent multidisciplinary oceanographic campaigns
861 between 2019 and 2022. IAVCEI Scientific Assembly, Rotorua, New-Zealand.
- 862 Le Losq, C., Cicconi, M.R., Neuville, D.R., 2021. Iron in Silicate Glasses and Melts:
863 Implications for Volcanological Processes, in: Moretti, R., Neuville, D.R. (Eds.),
864 Geophysical Monograph Series. Wiley, pp. 233–253.
865 <https://doi.org/10.1002/9781119473206.ch12>
- 866 Le Losq, C., Mysen, B.O., Cody, G.D., 2015a. Water and magmas: insights about the water
867 solution mechanisms in alkali silicate melts from infrared, Raman, and ²⁹Si solid-state
868 NMR spectroscopies. *Prog. Earth Planet. Sci.* 2, 22. [https://doi.org/10.1186/s40645-](https://doi.org/10.1186/s40645-015-0052-7)
869 [015-0052-7](https://doi.org/10.1186/s40645-015-0052-7)
- 870 Le Losq, C., Neuville, D.R., 2017. Molecular structure, configurational entropy and viscosity
871 of silicate melts: Link through the Adam and Gibbs theory of viscous flow. *J. Non-*
872 *Cryst. Solids* 463, 175–188. <https://doi.org/10.1016/j.jnoncrysol.2017.02.010>
- 873 Le Losq, C., Neuville, D.R., 2013. Effect of the Na/K mixing on the structure and the rheology
874 of tectosilicate silica-rich melts. *Chem. Geol.* 346, 57–71.
875 <https://doi.org/10.1016/j.chemgeo.2012.09.009>
- 876 Le Losq, C., Neuville, D.R., Florian, P., Henderson, G.S., Massiot, D., 2014. The role of Al³⁺
877 on rheology and structural changes in sodium silicate and aluminosilicate glasses and
878 melts. *Geochim. Cosmochim. Acta* 126, 495–517.
879 <https://doi.org/10.1016/j.gca.2013.11.010>
- 880 Le Losq, C., Neuville, D.R., Moretti, R., Kyle, P.R., Oppenheimer, C., 2015b. Rheology of
881 phonolitic magmas – the case of the Erebus lava lake. *Earth Planet. Sci. Lett.* 411, 53–
882 61. <https://doi.org/10.1016/j.epsl.2014.11.042>
- 883 Lejeune, A.M., Bottinga, Y., Trull, T.W., Richet, P., 1999. Rheology of bubble-bearing
884 magmas. *Earth Planet. Sci. Lett.* 166, 71–84. [https://doi.org/10.1016/S0012-](https://doi.org/10.1016/S0012-821X(98)00278-7)
885 [821X\(98\)00278-7](https://doi.org/10.1016/S0012-821X(98)00278-7)
- 886 Lejeune, A.-M., Richet, P., 1995. Rheology of crystal-bearing silicate melts: An experimental
887 study at high viscosities. *J. Geophys. Res. Solid Earth* 100, 4215–4229.
888 <https://doi.org/10.1029/94JB02985>
- 889 Lemoine, A., Briole, P., Bertil, D., Roullé, A., Foumelis, M., Thinon, I., Raucoules, D., de
890 Michele, M., Valtý, P., Hoste Colomer, R., 2020. The 2018–2019 seismo-volcanic
891 crisis east of Mayotte, Comoros islands: seismicity and ground deformation markers of
892 an exceptional submarine eruption. *Geophys. J. Int.* 223, 22–44.
893 <https://doi.org/10.1093/gji/ggaa273>
- 894 Liebske, C., Behrens, H., Holtz, F., Lange, R.A., 2003. The influence of pressure and
895 composition on the viscosity of andesitic melts. *Geochim. Cosmochim. Acta* 67, 473–
896 485. [https://doi.org/10.1016/S0016-7037\(02\)01139-0](https://doi.org/10.1016/S0016-7037(02)01139-0)

897 Le Losq, C., 2018. Rampy: a Python library for processing spectroscopic (IR, Raman, XAS...) data. <https://doi.org/10.5281/ZENODO.1168729>

898

899 Le Losq, C., and Neuville, D.R. (2013) Effect of the Na/K mixing on the structure and the rheology of tectosilicate silica-rich melts. *Chemical Geology*, 346, 57–71.

900

901 Le Losq, C., Neuville, D.R., Florian, P., Henderson, G.S., and Massiot, D. (2014) The role of Al³⁺ on rheology and structural changes in sodium silicate and aluminosilicate glasses and melts. *Geochimica et Cosmochimica Acta*, 126, 495–517.

902

903

904 Le Losq, C., Neuville, D.R., Moretti, R., Kyle, P.R., and Oppenheimer, C. (2015a) Rheology of phonolitic magmas – the case of the Erebus lava lake. *Earth and Planetary Science Letters*, 411, 53–61.

905

906

907 Le Losq, C., Mysen, B.O., and Cody, G.D. (2015b) Water and magmas: insights about the water solution mechanisms in alkali silicate melts from infrared, Raman, and ²⁹Si solid-state NMR spectroscopies. *Progress in Earth and Planetary Science*, 2, 22

908

909

910 Le Losq, C. and Neuville, D.R. (2017) Molecular structure, configurational entropy and viscosity of silicate melts: Link through the Adam and Gibbs theory of viscous flow. *Journal of Non-Crystalline Solids*, 463, 175–188.

911

912

913 Le Losq, C. (2018) Rampy: a Python library for processing spectroscopic (IR, Raman, XAS...) data. Zenodo.

914

915 Le Losq, C., Cicconi, M.R., and Neuville, D.R. (2021) Iron in Silicate Glasses and Melts: Implications for Volcanological Processes. In R. Moretti and D.R. Neuville, Eds., *Geophysical Monograph Series* pp. 233–253. Wiley.

916

917

918 Lejeune, A.-M., and Richet, P. (1995) Rheology of crystal-bearing silicate melts: An experimental study at high viscosities. *Journal of Geophysical Research: Solid Earth*, 100, 4215–4229.

919

920

921 Lejeune, A.M., Bottinga, Y., Trull, T.W., and Richet, P. (1999) Rheology of bubble-bearing magmas. *Earth and Planetary Science Letters*, 166, 71–84.

922

923 Lemoine, A., Briole, P., Bertil, D., Roullé, A., Foumelis, M., Thinon, I., Raucoules, D., de Michele, M., Valtý, P., and Hoste Colomer, R. (2020) The 2018–2019 seismo-volcanic crisis east of Mayotte, Comoros islands: seismicity and ground deformation markers of an exceptional submarine eruption. *Geophysical Journal International*, 223, 22–44.

924

925

926

927 Liebske, C., Behrens, H., Holtz, F., and Lange, R.A. (2003) The influence of pressure and composition on the viscosity of andesitic melts. *Geochimica et Cosmochimica Acta*, 67, 473–485.

928

929

930 Llewellyn, E.W., Manga, M., 2005. Bubble suspension rheology and implications for conduit flow. *J. Volcanol. Geotherm. Res.* 143, 205–217.

931

932 <https://doi.org/10.1016/j.jvolgeores.2004.09.018>

933 Ma, S., Zhang, X., Morrow, N.R., 1999. Influence of Fluid Viscosity On Mass Transfer Between Rock Matrix And Fractures. *J. Can. Pet. Technol.* 38.

934

935 <https://doi.org/10.2118/99-07-02>

- 936 Mader, H.M., Llewellyn, E.W., Mueller, S.P., 2013. The rheology of two-phase magmas: A
937 review and analysis. *J. Volcanol. Geotherm. Res.* 257, 135–158.
938 <https://doi.org/10.1016/j.jvolgeores.2013.02.014>
- 939 Malinovsky, V.K., Sokolov, A.P., 1986. The nature of boson peak in Raman scattering in
940 glasses. *Solid State Commun.* 57, 757–761. [https://doi.org/10.1016/0038-](https://doi.org/10.1016/0038-1098(86)90854-9)
941 [1098\(86\)90854-9](https://doi.org/10.1016/0038-1098(86)90854-9)
- 942 McClinton, J.T., White, S.M., Colman, A., Rubin, K.H., Sinton, J.M., 2014. The role of
943 crystallinity and viscosity in the formation of submarine lava flow morphology. *Bull.*
944 *Volcanol.* 76, 854. <https://doi.org/10.1007/s00445-014-0854-2>
- 945 McMillan, P., 1984. Structural studies of silicate glasses and melts—applications and
946 limitations of Raman spectroscopy. *Am. Mineral.* 69, 622–644.
- 947 Moitra, P., Gonnermann, H.M., Houghton, B.F., Tiwary, C.S., 2018. Fragmentation and Plinian
948 eruption of crystallizing basaltic magma. *Earth Planet. Sci. Lett.* 500, 97–104.
949 <https://doi.org/10.1016/j.epsl.2018.08.003>
- 950 Moretti, R., 2005. Polymerisation, basicity, oxidation state and their role in ionic modelling of
951 silicate melts. *Annals of Geophysics.*
- 952 Moretti, R., Le Losq, C., Neuville, D.R., 2014. The amphoteric behavior of water in silicate
953 melts from the point of view of their ionic-polymeric constitution. *Chem. Geol.* 367,
954 23–33. <https://doi.org/10.1016/j.chemgeo.2013.12.012>
- 955 Myers, M.L., Druitt, T.H., Schiavi, F., Gurioli, L., Flaherty, T., 2021. Evolution of magma
956 decompression and discharge during a Plinian event (Late Bronze-Age eruption,
957 Santorini) from multiple eruption-intensity proxies. *Bull. Volcanol.* 83, 18.
958 <https://doi.org/10.1007/s00445-021-01438-3>
- 959 Mysen, B., 1995. Experimental, in situ, high-temperature studies of properties and structure of
960 silicate melts relevant to magmatic processes. *Eur. J. Mineral.* 7, 745–766.
961 <https://doi.org/10.1127/ejm/7/4/0745>
- 962 Mysen, B., Richet, P., 2005. *Silicate Glasses and Melts*, Elsevier. ed, *Developments in*
963 *Geochemistry*. Amsterdam, Netherlands.
- 964 Mysen, B.O., Cody, G.D., 2005. Solution mechanisms of H₂O in depolymerized peralkaline
965 melts. *Geochim. Cosmochim. Acta* 69, 5557–5566.
966 <https://doi.org/10.1016/j.gca.2005.07.020>
- 967 Mysen, B.O., Richet, P., 2019. *Silicate Glasses and Melts*. Elsevier.
968 <https://doi.org/10.1016/C2018-0-00864-6>
- 969 Mysen, B.O., Richet, P., 2005. *Silicate glasses and melts: properties and structure*, 1st ed. ed,
970 *Developments in geochemistry*. Elsevier, Amsterdam ; Boston.
- 971 Mysen, B.O., Virgo, D., Scarfe, C.M., 1980. Relations between the anionic structure and
972 viscosity of silicate melts—a Raman spectroscopic study. *Am. Mineral.* 65, 690–710.

973 Mysen, B.O., Virgo, D., Scarfe, C.M., Cronin, D.J., 1985. Viscosity and structure of iron- and
974 aluminum-bearing calcium silicate melts at 1 atm. *Am. Mineral.* 70, 487–498.

975 Mysen, B.O., Virgo, D., Seifert, F.A., 1982. The structure of silicate melts: Implications for
976 chemical and physical properties of natural magma. *Rev. Geophys.* 20, 353.
977 <https://doi.org/10.1029/RG020i003p00353>

978 Nascimento, M.L.F., Aparicio, C., 2007. Data classification with the Vogel–Fulcher–
979 Tamman–Hesse viscosity equation using correspondence analysis. *Phys. B Condens.*
980 *Matter* 398, 71–77. <https://doi.org/10.1016/j.physb.2007.04.074>

981 Neuville, D.R., 2006. Viscosity, structure and mixing in (Ca, Na) silicate melts. *Chem. Geol.*
982 229, 28–41. <https://doi.org/10.1016/j.chemgeo.2006.01.008>

983 Neuville, D.R., Le Losq, C., 2022. Link between Medium and Long-range Order and
984 Macroscopic Properties of Silicate Glasses and Melts. *Rev. Mineral. Geochem.* 87,
985 105–162. <https://doi.org/10.2138/rmg.2022.87.03>

986 Neuville, D.R., Richet, P., 1991. Viscosity and mixing in molten (Ca, Mg) pyroxenes and
987 garnets. *Geochim. Cosmochim. Acta* 55, 1011–1019. [https://doi.org/10.1016/0016-](https://doi.org/10.1016/0016-7037(91)90159-3)
988 [7037\(91\)90159-3](https://doi.org/10.1016/0016-7037(91)90159-3)

989 Papale, P., 1999. Strain-induced magma fragmentation in explosive eruptions. *Nature* 397,
990 425–428. <https://doi.org/10.1038/17109>

991 Pelleter, A.-A., Caroff, M., Cordier, C., Bachelery, P., Nehlig, P., Debeuf, D., Arnaud, N.,
992 2014. Melilite-bearing lavas in Mayotte (France): An insight into the mantle source
993 below the Comores. *Lithos* 208–209, 281–297.
994 <https://doi.org/10.1016/j.lithos.2014.09.012>

995 Pistolesi, M., Rosi, M., Cioni, R., Cashman, K.V., Rossotti, A., Aguilera, E., 2011. Physical
996 volcanology of the post-twelfth-century activity at Cotopaxi volcano, Ecuador:
997 Behavior of an andesitic central volcano. *Geol. Soc. Am. Bull.* 123, 1193–1215.
998 <https://doi.org/10.1130/B30301.1>

999 Poole, J.P., 1949. LOW-TEMPERATURE VISCOSITY OF ALKALI SILICATE GLASSES.
1000 *J. Am. Ceram. Soc.* 32, 230–233. <https://doi.org/10.1111/j.1151-2916.1949.tb18952.x>

1001 Popa, R.-G., Bachmann, O., Huber, C., 2021. Explosive or effusive style of volcanic eruption
1002 determined by magma storage conditions. *Nat. Geosci.* 14, 781–786.
1003 <https://doi.org/10.1038/s41561-021-00827-9>

1004 Prival, J.-M., 2021. On the emplacement dynamics of viscous, silicic lava flows. Université
1005 Clermont Auvergne, France.

1006 Puzenat V., Feuillet N., Komorowski J-C., Escartin J., Deplus C. , Bachèlery P. , Berthod C. ,
1007 Gurioli L., Scalabrin C., Cathalot C., and others (2022) Volcano-tectonic structures of
1008 Mayotte’s upper submarine slope: insights from high-resolution bathymetry and in-situ
1009 imagery from a deep towed camera. **Submitted to Comptes Rendus Geoscience,**
1010 **Special issue.**

- 1011 REVOSIMA (2022) Campagne MD239-MAYOBS23 : Note finale. Vendredi 23 Juillet 2022
1012 https://www.ipgp.fr/sites/default/files/md239-mayobs23_note-finale_20220727.pdf
- 1013 Richet, P., 1984. Viscosity and configurational entropy of silicate melts. *Geochim.*
1014 *Cosmochim. Acta* 48, 471–483. [https://doi.org/10.1016/0016-7037\(84\)90275-8](https://doi.org/10.1016/0016-7037(84)90275-8)
- 1015 Rinnert E., Lebas E., Jorry S., Feuillet N., Thinon I., Fouquet Y. (2019) MAYOBS,
1016 <https://doi.org/10.18142/291>
- 1017 Robert, G., Smith, R.A., Whittington, A.G., 2019. Viscosity of melts in the NaAlSiO₄-
1018 KAlSiO₄-SiO₂ system: Configurational entropy modelling. *J. Non-Cryst. Solids* 524,
1019 119635. <https://doi.org/10.1016/j.jnoncrysol.2019.119635>
- 1020 Scarfe, C., Mysen, B.O., Virog, D., 1987. Pressure dependence of the viscosity of silicate melts.
1021 *Magmat. Process. Physicochem. Princip* 59–67.
- 1022 Scheu, B., Dingwell, D.B., 2022. Magma Fragmentation. *Rev. Mineral. Geochem.* 87, 767–
1023 800. <https://doi.org/10.2138/rmg.2021.87.16>
- 1024 Schiavi, F., Bolfan-Casanova, N., Withers, A.C., Médard, E., Laumonier, M., Laporte, D.,
1025 Flaherty, T., Gómez-Ulla, A., 2018. Water quantification in silicate glasses by Raman
1026 spectroscopy: Correcting for the effects of confocality, density and ferric iron. *Chem.*
1027 *Geol.* 483, 312–331. <https://doi.org/10.1016/j.chemgeo.2018.02.036>
- 1028 Shaw, H.R., 1972. Viscosities of magmatic silicate liquids; an empirical method of prediction.
1029 *Am. J. Sci.* 272, 870–893. <https://doi.org/10.2475/ajs.272.9.870>
- 1030 Shea, T., Hellebrand, E., Gurioli, L., Tuffen, H., 2014. Conduit- to Localized-scale Degassing
1031 during Plinian Eruptions: Insights from Major Element and Volatile (Cl and H₂O)
1032 Analyses within Vesuvius AD 79 Pumice. *J. Petrol.* 55, 315–344.
1033 <https://doi.org/10.1093/petrology/egt069>
- 1034 SHOM, 2016. MNT bathymetrique de la façade de Mayotte (Projet
1035 Homonim). http://dx.doi.org/10.17183/MNT_MAY100m_HOMONIM_WGS84
- 1036 Spera, F.J., Borgia, A., Strimple, J., Feigenson, M., 1988. Rheology of melts and magmatic
1037 suspensions: 1. Design and calibration of concentric cylinder viscometer with
1038 application to rhyolitic magma. *J. Geophys. Res. Solid Earth* 93, 10273–10294.
1039 <https://doi.org/10.1029/JB093iB09p10273>
- 1040 Starodub, K., Wu, G., Yazhenskikh, E., Müller, M., Khvan, A., Kondratiev, A., 2019. An
1041 Avramov-based viscosity model for the SiO₂-Al₂O₃-Na₂O-K₂O system in a wide
1042 temperature range. *Ceram. Int.* 45, 12169–12181.
1043 <https://doi.org/10.1016/j.ceramint.2019.03.121>
- 1044 Stebbins, J.F., Farnan, I., Xue, X., 1992. The structure and dynamics of alkali silicate liquids:
1045 A view from NMR spectroscopy. *Chem. Geol.* 96, 371–385.
1046 [https://doi.org/10.1016/0009-2541\(92\)90066-E](https://doi.org/10.1016/0009-2541(92)90066-E)
- 1047 Stebbins, J.F., Xu, Z., 1997. NMR evidence for excess non-bridging oxygen in an
1048 aluminosilicate glass. *Nature* 390, 60–62. <https://doi.org/10.1038/36312>

- 1049 Takahashi, Y., Osada, M., Masai, H., Fujiwara, T., 2009. Crystallization and nanometric
1050 heterogeneity in glass: *In situ* observation of the boson peak during crystallization.
1051 Phys. Rev. B 79, 214204. <https://doi.org/10.1103/PhysRevB.79.214204>
- 1052 Tammann, G., Hesse, W., 1926. Die Abhängigkeit der Viscosität von der Temperatur bei
1053 unterkühlten Flüssigkeiten. Z. Für Anorg. Allg. Chem. 156, 245–257.
1054 <https://doi.org/10.1002/zaac.19261560121>
- 1055 Thomas, N., Jaupart, C., Vergnolle, S., 1994. On the vesicularity of pumice. J. Geophys. Res.
1056 99, 15633. <https://doi.org/10.1029/94JB00650>
- 1057 Vogel, D.H., 1921. Das Temperaturabhängigkeitsgesetz der Viskosität von Flüssigkeiten.
1058 Physikalische Zeitschrift 22, 645.
- 1059 Wadsworth, F.B., Witcher, T., Vossen, C.E.J., Hess, K.-U., Unwin, H.E., Scheu, B., Castro,
1060 J.M., Dingwell, D.B., 2018. Combined effusive-explosive silicic volcanism straddles
1061 the multiphase viscous-to-brittle transition. Nat. Commun. 9, 4696.
1062 <https://doi.org/10.1038/s41467-018-07187-w>
- 1063 Whittington, A., Richet, P., Holtz, F., 2000. Water and the viscosity of depolymerized
1064 aluminosilicate melts. Geochim. Cosmochim. Acta 64, 3725–3736.
1065 [https://doi.org/10.1016/S0016-7037\(00\)00448-8](https://doi.org/10.1016/S0016-7037(00)00448-8)
- 1066 Whittington, A., Richet, P., Linard, Y., Holtz, F., 2001. The viscosity of hydrous phonolites
1067 and trachytes. Chem. Geol. 174, 209–223. [https://doi.org/10.1016/S0009-2541\(00\)00317-X](https://doi.org/10.1016/S0009-2541(00)00317-X)
- 1069 Xue, X., Kanzaki, M., 2006. Depolymerization effect of water in aluminosilicate glasses:
1070 Direct evidence from ¹H-²⁷Al heteronuclear correlation NMR. Am. Mineral. 91,
1071 1922–1926. <https://doi.org/10.2138/am.2006.2365>
- 1072 Xue, X., Kanzaki, M., 2004. Dissolution mechanisms of water in depolymerized silicate melts:
1073 Constraints from ¹H and ²⁹Si NMR spectroscopy and ab initio calculations. Geochim.
1074 Cosmochim. Acta 68, 5027–5057. <https://doi.org/10.1016/j.gca.2004.08.016>
- 1075 Zhang, Y., Ni, H., 2010. Diffusion of H, C, and O Components in Silicate Melts. Rev. Mineral.
1076 Geochem. 72, 171–225. <https://doi.org/10.2138/rmg.2010.72.5>
- 1077